

Efficient two-color Floquet control of the RKKY interaction in altermagnets

Mohsen Yarmohammadi^{1*}, Pei-Hao Fu² and James K. Freericks¹

¹ Department of Physics, Georgetown University, Washington DC 20057, USA

² Department of Physics and Astronomy, University of Florence, I-50019 Sesto Fiorentino, Italy

* mohsen.yarmohammadi@georgetown.edu

Abstract

Magnetic impurities in real materials can mask the intrinsic spin-dependent properties of hosts. They interact indirectly through the Ruderman–Kittel–Kasuya–Yosida (RKKY) mechanism, which limits the use of isolated impurity spins in applications such as qubits and spintronics. By suppressing the RKKY interaction, an effective control scheme should therefore enable access to the host’s unperturbed behavior while simultaneously isolating the impurity spins for functional use. Although beyond static approaches, single-color laser driving can suppress the RKKY interaction, it typically requires strong fields that may be impractical or destabilizing. To overcome these limitations, we show that two-color laser driving provides efficient and tunable control over all components of the RKKY interaction using two weak laser fields. Focusing on two-dimensional Rashba altermagnets, we show that interference between one- and two-photon processes produces altermagnet-specific Floquet corrections. These include additional AC Stark shifts, magnetizations, spin–orbit renormalization, and emergent in-plane Zeeman fields, which are absent under single-color driving and in non-altermagnetic systems. Notably, two-color driving induces a finite z -component of the Dzyaloshinskii–Moriya (DM) interaction, stabilizing in-plane chiral magnetism and related textures in Rashba altermagnets. These effects enable tunable, near-complete on–off switching of the Heisenberg, Ising, and DM interactions through a Lifshitz-like modulation of the Fermi surface. We also show that the tuning process is highly sensitive to the chirality of both beams. We further map out phase diagrams for ferromagnetic and antiferromagnetic alignment of impurities with clockwise and counterclockwise canting as a function of Rashba coupling and altermagnetic order. Finally, we discuss candidate material platforms and experimental feasibility.

Contents

1	Introduction	2
2	Hamiltonian model	3
3	Magnetic impurities and the RKKY interaction	8
4	Results and discussion	9
5	Experimental relevance and material platforms	16

6 Summary and outlook	16
References	17

1 Introduction

Altermagnets are a recently identified class of magnetic materials [1–4] whose electronic bands exhibit momentum-dependent spin splitting despite vanishing net magnetization. Unlike ferromagnets, where spin splitting arises from uniform magnetization, or conventional antiferromagnets, where combined symmetries enforce spin degeneracy in momentum space, altermagnets host spin-polarized bands with spin polarization that changes sign across the Brillouin zone [1–11]. This distinct symmetry structure gives rise to unconventional transport and optical responses [12–15], including charge–spin conversion [16], giant and tunneling magnetoresistance [9], anomalous Hall effects [5, 17, 18], nonlinear transport [19], spin filtering effects [13, 20–28] among other phenomena [29–33], while maintaining magnetic compensation. Altermagnets therefore provide a promising platform for spintronic functionalities without macroscopic magnetization [34–37].

Because the defining property of altermagnets lies in the momentum-resolved spin structure of their electronic states [18, 38–41], it is natural to ask how this spin texture influences magnetic interactions mediated by itinerant electrons. Magnetic impurities embedded in metallic hosts provide a transparent platform for addressing this question. In particular, the Ruderman–Kittel–Kasuya–Yosida (RKKY) interaction [42–46] generates an indirect exchange between spatially separated local spins and is highly sensitive to the host band structure, Fermi-surface geometry, and spin-dependent correlations. Analyzing the RKKY interaction, therefore, provides direct insight into how altermagnetic spin textures reshape impurity-mediated magnetic coupling at the nanoscale [45, 45–49].

Rashba altermagnets, where Rashba spin–orbit coupling (RSOC) coexists with altermagnetic order, offer a versatile platform for engineering spin-dependent interactions. While the RKKY interaction in these systems is highly anisotropic and tunable [46, 47, 49], controllable on–off switching remains challenging. Magnetic impurities in real materials inevitably obscure their intrinsic behavior. To accurately probe the host’s fundamental behavior, it is therefore important to minimize or account for their influence while recognizing that the impurities cannot be eliminated. On the other hand, although RKKY-mediated exchange between impurities can stabilize collective magnetic phases, its long-range nature often masks single-impurity physics. Individual magnetic impurities are technologically significant, acting as addressable quantum spins in quantum information science [50, 51], as ultrasensitive nanoscale sensors [52–54], and as functional elements in spintronic memory devices [55, 56]. Suppressing RKKY coupling enables effectively decoupled local spins, opening the door to single-spin applications.

Given this background, an efficient control strategy is essential both to (i) extract pristine information from the altermagnet in realistic experimental setups with dilute magnetic impurities and (ii) decouple individual magnetic impurities for single-spin device applications. In this context, dynamical control via external periodic driving offers a reversible route to tuning indirect exchange beyond static limitations [46, 57]. Optical control of the RKKY interaction has been explored in various nonequilibrium settings [47, 58–62], including Floquet-engineered band renormalization and magnetizing the system. However, under monochromatic driving, achieving such control generally requires strong fields to appreciably modify the Fermi-level states, which are necessary for efficient tuning of the RKKY interaction to either decouple magnetic impurities or reveal the intrinsic host properties. This requirement, in turn, limits

both the efficiency and robustness of the approach. These limitations motivate the exploration of alternative driving protocols that can reshape the electronic structure more efficiently, enabling control over the RKKY interaction and impurity decoupling without requiring excessively strong fields that risk destabilizing the system.

In this work, we demonstrate that bichromatic driving [63–74] provides precisely such a mechanism in altermagnets. In particular, we propose a two-color laser driving protocol in two-dimensional (2D) Rashba altermagnets, using two weak laser beams instead of a single strong beam. The coherent fields, with distinct frequencies, phases, chiralities, and amplitudes, provide enhanced control over Floquet band hybridization and momentum-resolved spin polarization. This enables a much stronger on–off switching process—and in some regimes complete cancellation—of RKKY tensor components compared to monochromatic driving [47]. While the mechanism we consider is generally applicable to a broad class of altermagnetic wave patterns—including d -, g -, f -, and i -wave forms [1–3, 6, 8, 75]—we focus here on d -wave altermagnets, which have been predicted to host a variety of unconventional current-driven spin phenomena, such as exotic spin torques, spin–orbit torques, and spin-splitter currents [17, 34].

The remainder of this paper is organized as follows. In Sec. 2, we introduce the model Hamiltonian for 2D Rashba altermagnets and describe the two-color laser driving protocol. In Sec. 3, we present the theoretical framework for evaluating the laser-modified RKKY interaction between magnetic impurities. Section 4 contains numerical results illustrating on–off switching of RKKY interaction across a range of model parameters. Section 5 provides experimental relevance and candidate materials. Finally, Sec. 6 summarizes our findings and briefly outlines prospects for future studies.

2 Hamiltonian model

We consider a 2D Rashba d -wave altermagnet described by a minimal tight-binding model capturing kinetic energy, RSOC, and altermagnetic exchange. We employ a quadratic continuum model valid near the Γ point. In equilibrium, these terms generate momentum-dependent spin splitting while preserving zero net magnetization. External periodic driving, as shown in Fig. 1, is incorporated to dynamically reshape the electronic structure and, in turn, the impurity-mediated RKKY interaction later. The equilibrium Hamiltonian is given by $H_d = H_{\text{kin}} + H_R + H_{\text{AM}}$, where H_{kin} describes the parabolic band dispersion, H_R the RSOC of strength λ_R , and H_{AM} the altermagnetic exchange characterized by M_d . Thus, the bare conduction electrons in a 2D Rashba altermagnet are described by

$$H_d(\mathbf{k}) = \varepsilon(k_x^2 + k_y^2)\sigma_0 + \lambda_R(k_x\sigma_y - k_y\sigma_x) + M_{\mathbf{k}}^d\sigma_z, \quad (1)$$

where $\varepsilon = \hbar^2/2m_e$ is the band mass term. The last term,

$$M_{\mathbf{k}}^d = \frac{\hbar^2 M_d}{m_e} \left[\frac{(k_x^2 - k_y^2)}{2} \cos(2\theta_M^d) + k_x k_y \sin(2\theta_M^d) \right], \quad (2)$$

represents the momentum-dependent altermagnetic exchange splitting characteristic of d -wave altermagnets. The angle θ_M^d rotates the d -wave texture in the Brillouin zone: $\theta_M^d = 0$ corresponds to a $d_{x^2-y^2}$ -type altermagnetic pattern, while $\theta_M^d = \pi/4$ corresponds to a d_{xy} -type pattern. The Rashba term induces in-plane spin–momentum locking, with spins oriented perpendicular to momentum $(\mathbf{k} \times \boldsymbol{\sigma})_z$, underpinning spin textures and transport. In contrast, the altermagnetic term $M_{\mathbf{k}}^d\sigma_z$ vanishes along symmetry lines, and changes sign between opposite momentum sectors, yielding a compensated, noncollinear spin texture in \mathbf{k} -space with zero net magnetization—the hallmark of altermagnets. Their interplay produces a highly anisotropic momentum-space spin texture.

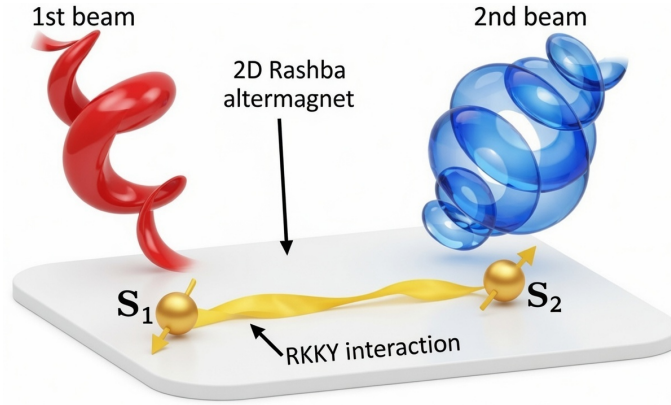


Figure 1: Schematic illustration of two-color Floquet engineering of the RKKY interaction in a 2D Rashba altermagnet. Two coherent laser beams irradiate the system, with frequencies ω_1 and ω_2 , amplitudes A_0 and SA_0 (where S denotes the relative strength of the second-harmonic component), phases ϕ_1 and ϕ_2 , and chiralities η_1 and η_2 . Two localized magnetic moments, \mathbf{S}_1 and \mathbf{S}_2 , interact indirectly via the laser-modified itinerant electrons, yielding a tunable RKKY exchange. The relative amplitude ratio and chirality of the beams control the strength, anisotropy, and components of the RKKY coupling.

Although the system is intrinsically a Rashba altermagnet and already exhibits rich equilibrium properties, external light irradiation offers a versatile and controllable route to further tailor its electronic and spin structure beyond static limitations. In particular, time-periodic driving can dynamically renormalize the band dispersion, spin splitting, and symmetry characteristics without modifying the underlying lattice. Optical excitation can selectively break or reshape discrete symmetries, generate effective spin–orbit fields, and produce nonequilibrium spin textures that do not arise in equilibrium. In this way, light acts as an external tuning parameter for manipulating altermagnetic spin-dependent phenomena in situ, enabling controlled modification of exchange interactions and magnetic anisotropies.

Although various driving protocols involving linearly polarized fields, or mixed circular and linear polarization, can in principle be considered, we focus here on two circularly polarized lights for physical clarity and minimality. In a 2D Rashba altermagnet, circularly polarized light dynamically breaks time-reversal symmetry and introduces a well-defined chirality, which is essential for activating Floquet-induced exchange channels beyond simple parameter renormalization [47, 62]. In contrast, linearly polarized driving preserves an effective time-reversal symmetry over one period and predominantly leads to anisotropic band renormalization without generating qualitatively new interaction terms. Mixed circular–linear schemes produce intermediate effects that can be understood as subsets of the circular–circular case. Thus, two circularly polarized fields constitute the minimal optical configuration that captures the full symmetry-allowed Floquet control of a Rashba altermagnet.

Accordingly, the system is driven by two circularly polarized laser fields, incorporated via the Peierls substitution $\mathbf{k} \rightarrow \mathbf{k} + e\mathbf{A}(t)/\hbar$. The coupling to the electromagnetic field enters through the vector potential $\mathbf{A}(t) = (A_x(t), A_y(t))$ with

$$A_x(t) = A_0[\eta_1 \cos(\omega t) + \eta_2 S \cos(n\omega t + \phi)], \quad (3a)$$

$$A_y(t) = A_0[\eta_1 \sin(\omega t) + \eta_2 S \sin(n\omega t + \phi)]. \quad (3b)$$

In this formulation, the dimensionless ratio S parametrizes the relative strength of the second harmonic component. The factors $\eta_{1,2}$ encode the chirality of the two laser fields, while n and $\phi = \phi_2 - \phi_1$ denote the frequency ratio and relative phase offset between the driving fields,

respectively. The amplitude of the vector potential is further defined as $A_0 = E_0/\omega$, where E_0 and ω denote the electric-field amplitude and frequency of the first laser beam, respectively. In equilibrium, the characteristic momentum-dependent spin splitting of altermagnets is protected by the combined $C_4\mathcal{T}$ symmetry. Optical driving modifies this symmetry structure. While linearly polarized light reduces rotational symmetry, circularly polarized light explicitly breaks $C_4\mathcal{T}$ due to its definite chirality.

Although the formalism developed here applies in principle to general bichromatic driving schemes of the form $\omega-n\omega$, we focus on the $\omega-2\omega$ configuration for the following concrete physical and experimental reasons. The second-harmonic component represents the simplest nonlinear extension beyond single-frequency driving and enables strong interference between single- and two-photon absorption pathways at moderate field strengths. This allows efficient symmetry control and Floquet-induced band mixing without requiring intense electromagnetic fields. Moreover, $\omega-2\omega$ driving couples naturally to even-parity and quadrupolar features of the band structure, making it particularly compatible with d -wave altermagnetic order. Experimentally, phase-coherent $\omega-2\omega$ laser setups are well established [63–67], offering precise control over relative phase, polarization, and intensity.

Since the Hamiltonian is periodic in time, $H_d(\mathbf{k}, t + 2\pi/\omega) = H_d(\mathbf{k}, t)$, the driven system can be analyzed using the high-frequency Floquet–Magnus expansion [76, 77], which maps the time-dependent problem onto an effective time-independent eigenvalue equation in an extended Hilbert space. Although periodic driving can, in principle, induce heating, we consider the off-resonant regime with weak driving amplitude, where the system is expected to enter a long-lived prethermal state that is accurately described by the effective Floquet Hamiltonian. In this regime, a controlled analytical treatment becomes possible. Accordingly, we set the driving frequency to $\hbar\omega \geq 1$ eV, exceeding the relevant low-energy electronic bandwidth. As a result, Floquet sidebands remain well separated, resonant crossings are suppressed, and photon-assisted interband transitions are negligible. This separation of energy scales allows averaging over the rapid micromotion induced by the periodic drive, yielding an effective static description in which energy absorption occurs perturbatively. We implement this procedure using the van Vleck inverse-frequency expansion [78–80], which provides a systematic perturbative construction of a time-independent Floquet Hamiltonian to leading order in $1/\omega$. Within this framework, the effective Hamiltonian is

$$\mathcal{H}_d^{\text{eff}}(\mathbf{k}) \approx \mathcal{H}_0^{\text{F}}(\mathbf{k}) + \frac{1}{\hbar\omega} [\mathcal{H}_{-1}^{\text{F}}(\mathbf{k}), \mathcal{H}_{+1}^{\text{F}}(\mathbf{k})], \quad (4)$$

where the Fourier components ($m = 0, \pm 1$) of the driven Hamiltonian are defined as

$$\mathcal{H}_m^{\text{F}}(\mathbf{k}) = \frac{\omega}{2\pi} \int_0^{\frac{2\pi}{\omega}} dt H_d(\mathbf{k} + e\mathbf{A}(t)/\hbar) e^{im\omega t}. \quad (5)$$

The resulting effective Hamiltonian governs the slow, stroboscopic dynamics of the driven system and faithfully captures its long-time behavior after averaging over rapid intra-period oscillations.

Substituting $\mathbf{k} \rightarrow \mathbf{k} + e\mathbf{A}(t)/\hbar$ in $H_d(\mathbf{k})$ via the minimal coupling scheme expands the Hamiltonian in powers of \mathbf{A} , leading to (we set $e = \hbar = 1$ for simplicity, but will restore them later)

$$\begin{aligned} H_d(\mathbf{k} + \mathbf{A}(t)) &= H_d(\mathbf{k}) + M_S^{\text{d}} \sigma_z A_x(t) A_y(t) + \left[2 \left(\varepsilon \sigma_0 + \frac{M_C^{\text{d}}}{2} \sigma_z \right) k_x + \lambda_{\text{R}} \sigma_y + M_S^{\text{d}} \sigma_z k_y \right] A_x(t) \\ &+ \left[2 \left(\varepsilon \sigma_0 - \frac{M_C^{\text{d}}}{2} \sigma_z \right) k_y - \lambda_{\text{R}} \sigma_x + M_S^{\text{d}} \sigma_z k_x \right] A_y(t) + \left(\varepsilon \sigma_0 + \frac{M_C^{\text{d}}}{2} \sigma_z \right) A_x^2(t) \\ &+ \left(\varepsilon \sigma_0 - \frac{M_C^{\text{d}}}{2} \sigma_z \right) A_y^2(t). \end{aligned} \quad (6)$$

For notational convenience, we introduce the coefficients

$$M_C^d \equiv M_d \cos(2\theta_M^d), \quad M_S^d \equiv M_d \sin(2\theta_M^d). \quad (7)$$

After straightforward integrals for $n = 2$ in both $A_x(t)$ and $A_y(t)$, we find

$$H_d^{\text{eff}}(\mathbf{k}) \approx H_d(\mathbf{k}) + \varepsilon A_0^2 (1 + S^2) \sigma_0 + \left(1 - \frac{S^2}{2}\right) \frac{[f_{-1}, f_{+1}]}{\omega} + \frac{3S}{2} \left(e^{-i\phi} \frac{[f_{+2}, f_{+1}]}{\omega} - e^{i\phi} \frac{[f_{-2}, f_{-1}]}{\omega} \right), \quad (8)$$

where

$$f_{+1} = \frac{A_0}{2} \left[2(\varepsilon \sigma_0 + M_C^d \sigma_z) k_x + \lambda_R \sigma_y + 2M_S^d \sigma_z k_y \right] + \frac{iA_0}{2} \left[2(\varepsilon \sigma_0 - M_C^d \sigma_z) k_y - \lambda_R \sigma_x + 2M_S^d \sigma_z k_x \right], \quad (9a)$$

$$f_{+2} = \frac{1}{2} A_0^2 (M_C^d + iM_S^d) \sigma_z, \quad (9b)$$

and $f_{\pm\ell} = f_{\mp\ell}^\dagger$ for $\ell = 1$ and 2 . The term proportional to $A_0^2(1 + S^2)\sigma_0$ represents a light-induced scalar (AC Stark) shift arising from second-order absorption–emission processes that rigidly shift the electronic spectrum. The commutator $[f_{-1}, f_{+1}]/\omega$ captures virtual single-photon processes at the fundamental frequency ω , renormalizing the RSOC and momentum-dependent altermagnetic exchange. Importantly, the additional terms $[f_{+2}, f_{+1}]$ and $[f_{-2}, f_{-1}]$ describe interference between virtual pathways involving one- and two-photon processes from the ω and 2ω components of the drive. In addition to the S -dependent contributions in the AC Stark and Rashba terms, these latter commutators emerge specifically under the two-color driving protocol. The relative phase ϕ and amplitude ratio S control constructive or destructive interference between these pathways, enabling selective enhancement or suppression of spin-dependent Floquet band hybridization.

Using Eqs. (8) and (9), and corresponding commutators, we obtain

$$H_d^{\text{eff}}(\mathbf{k}) = \left[\varepsilon (k_x^2 + k_y^2) + \mu_\omega \right] \sigma_0 + \left[(\lambda_R + \lambda_{R\omega}) k_x + \lambda_{D\omega} k_y \right] \sigma_y - \left[(\lambda_R - \lambda_{R\omega}) k_y + \lambda_{D\omega} k_x \right] \sigma_x + M_{\mathbf{k}}^d \sigma_z + \boldsymbol{\Omega} \cdot \boldsymbol{\sigma}, \quad (10)$$

with

$$\mu_\omega = \varepsilon A_0^2 (1 + S^2), \quad (11a)$$

$$\lambda_{R\omega} = \lambda_R M_C^d A_0^2 \frac{\eta_1 + \eta_2 S^2}{\hbar \omega}, \quad (11b)$$

$$\lambda_{D\omega} = \lambda_R M_S^d A_0^2 \frac{\eta_1 + \eta_2 S^2}{\hbar \omega}, \quad (11c)$$

$$\Omega_x = \frac{\lambda_R}{4\hbar\omega} A_0^3 S \left[M_C^d (2\eta_2 \eta_1 - 1) \sin(\phi) + 2M_S^d (\eta_1 - 2\eta_2) \cos(\phi) \right], \quad (11d)$$

$$\Omega_y = \frac{\lambda_R}{4\hbar\omega} A_0^3 S \left[2M_S^d (2 - \eta_2 \eta_1) \sin(\phi) + M_C^d (2\eta_1 - \eta_2) \cos(\phi) \right], \quad (11e)$$

$$\Omega_z = \frac{\lambda_R^2}{2} A_0^2 \frac{\eta_1 + \eta_2 S^2}{\hbar \omega}. \quad (11f)$$

Upon rewriting the effective Hamiltonian in the form $H_d^{\text{eff}}(\mathbf{k}) = h_0(\mathbf{k}) \sigma_0 + \mathbf{h}(\mathbf{k}) \cdot \boldsymbol{\sigma}$, the eigenvalues are readily obtained, giving rise to the upper and lower energy bands

$$E_\pm(\mathbf{k}) = h_0(\mathbf{k}) \pm |\mathbf{h}(\mathbf{k})|. \quad (12)$$

In the limit $S = 0$, the model reduces to monochromatic circularly polarized light [47, 62, 81, 82]. The momentum-linear terms σ_x and σ_y encode Floquet-modified spin–momentum locking: Rashba- and Dresselhaus-type terms, $\lambda_{R\omega}$ and $\lambda_{D\omega}$, arise from virtual single-photon processes that anisotropically renormalize the Rashba interaction in $d_{x^2-y^2}$ and d_{xy} altermagnets, respectively. Higher-order

Term	One-color	Two-color	W/O M_C^d	W/O M_S^d	W/O altermagnetism?
μ_ω	✓ (strong field)	✓ (weak fields)	✓	✓	✓
$\lambda_{R\omega}$	✓ (strong field)	✓ (weak fields)	✓	✗	✗
$\lambda_{D\omega}$	✓ (strong field)	✓ (weak fields)	✗	✓	✗
Ω_x	✗	✓	✗	✗	✗
Ω_y	✗	✓	✗	✗	✗
Ω_z	✓ (strong field)	✓ (weak fields)	✓	✓	✓

Table 1: Comparison of effective Floquet-induced terms and their efficiency for tuning the band structure under one-color and two-color laser driving. The last three columns summarize the dependence of Floquet-induced terms on the altermagnetic order parameters M_C^d and M_S^d to see how Hamiltonian terms appear without (W/O) altermagnetism.

multiphoton processes produce an effective Zeeman field $\mathbf{\Omega} \cdot \boldsymbol{\sigma}$, breaking time-reversal symmetry and generating momentum-independent spin splitting. These Floquet-induced terms vanish when $M_C^d = 0$ and $M_S^d = 0$, highlighting that such light responses are unique to altermagnets. In contrast, monochromatic circular driving preserves space–time rotational symmetry, forbidding static in-plane Zeeman fields $\Omega_x \sigma_x$ and $\Omega_y \sigma_y$. Among the Floquet-induced terms, $\lambda_{R\omega}$, $\lambda_{D\omega}$, and $\Omega_{x,y}$ play a key role in reshaping the Fermi surface, suppressing static spin susceptibility, and enhancing switching efficiency by activating additional RKKY channels.

Table 1 compares one- and two-color driving protocols. Monochromatic driving only provides rigid band shifts and magnetizations, which compete with Rashba and altermagnetic splittings and thus require strong fields to strongly reshape the Fermi surface for a Lifshitz-like transition. Bichromatic driving, in contrast, enables similar band-structure tuning at much lower peak intensities, making Floquet engineering both robust and experimentally practical. In particular, the decisive control channels $\Omega_{x,y}$ are absent in monochromatic driving and vanish without altermagnetic order. The last three columns show that while the scalar shift μ_ω and out-of-plane Zeeman-like field Ω_z persist without altermagnetism, all in-plane spin–orbit renormalizations and Zeeman-like fields require altermagnetic order, i.e., finite M_C^d and/or M_S^d .

Although in-plane Zeeman terms can arise from substrate-induced proximity effects [83–86], such approaches rely on static, material-specific interfaces that are fixed once fabricated. By contrast, two-color laser driving generates effective in-plane Zeeman-like fields intrinsically within the 2D Rashba altermagnet, allowing continuous, reversible, and symmetry-selective control via intensity, polarization, and relative phase. This optical route also avoids interface-induced disorder, uncontrolled hybridization, and additional symmetry breaking, providing a clean and versatile platform for engineering spin-dependent band structure effects beyond static heterostructures.

We have shown that the host electrons in Rashba altermagnets exhibit novel spin-dependent behavior under a two-color laser driving scheme. To understand how these emergent features manifest in realistic experimental conditions—where materials inevitably contain dilute impurities (both charged and magnetic)—we focus here on magnetic impurities, as the driven host system develops intrinsically spin-dependent electronic responses. Magnetic impurities act as localized spin probes that couple to the itinerant electrons via a local exchange interaction. In contrast to extended magnetic order, a dilute impurity carries a well-defined localized moment, enabling a controlled analysis of how the host electronic system mediates spin-dependent interactions. Consequently, magnetic impurities serve as tunable test spins whose effective coupling directly encodes the spin susceptibility and Fermi-surface properties of the underlying material. Studying their interaction therefore provides a minimal and direct framework for characterizing carrier-mediated magnetism, spin anisotropy, and the impact of spin–orbit coupling and external driving on the material structure. Moreover, a single impurity only induces a local spin polarization of the conduction electrons, whereas the effective magnetic coupling emerges when the spin density generated by one impurity interacts with a second spatially separated impurity. The two-impurity configuration, therefore, represents the minimal and most transparent setup to extract the

carrier-mediated exchange interaction and to analyze how its range, oscillation period, and anisotropy are modified by the Floquet-renormalized Rashba–altermagnetic band structure.

3 Magnetic impurities and the RKKY interaction

We consider two localized magnetic moments, \mathbf{S}_1 and \mathbf{S}_2 , as shown in Fig. 1. They are separated by the vector \mathbf{R} and the relative angle φ_R . The impurity spins are coupled to the itinerant electrons via a local exchange interaction

$$H_{\text{sd}} = J_{\text{sd}} \sum_{i=1,2} \mathbf{S}_i \cdot \mathbf{s}(\mathbf{R}_i), \quad (13)$$

where $\mathbf{s}(\mathbf{r}) = \frac{1}{2} c^\dagger(\mathbf{r}) \boldsymbol{\sigma} c(\mathbf{r})$ is the electron spin density and J_{sd} denotes the exchange coupling strength, typically lying in the range 10 meV to 1 eV in metallic and semiconducting hosts [87–89]. In the weak-coupling regime, the interaction between impurities arises at second order in J_{sd} upon integrating out the itinerant electrons, yielding the RKKY interaction. Since the electronic system is periodically driven, the exchange interaction is evaluated using the static component of the Rashba-Floquet Green’s function derived from the effective Hamiltonian. The effective RKKY Hamiltonian takes the most general bilinear form

$$H_{\text{RKKY}} = \sum_{\alpha, \beta=x, y, z} J_{\alpha\beta}(\mathbf{R}) S_1^\alpha S_2^\beta, \quad J_{\alpha\beta}(\mathbf{R}) = -J_{\text{sd}}^2 \chi_{\alpha\beta}(\mathbf{R}). \quad (14)$$

The static spin susceptibility of the host material is expressed as

$$\chi_{\alpha\beta}(\mathbf{R}) = -\frac{1}{\pi} \int_{-\infty}^{\mu} dE \text{Im} [\text{Tr} (\sigma_\alpha G(\mathbf{R}, E) \sigma_\beta G(-\mathbf{R}, E))], \quad (15)$$

where

$$G(\mathbf{R}, E) = \int \frac{d^2\mathbf{k}}{(2\pi)^2} \frac{e^{i\mathbf{k}\cdot\mathbf{R}}}{E - H_{\text{d}}^{\text{eff}}(\mathbf{k}) + i0^+} \quad (16)$$

is the retarded Floquet Green’s function of the Rashba altermagnet in real space, and μ denotes the Fermi energy, which coincides with the chemical potential in the zero temperature limit assumed throughout this work. The $H_{\text{d}}^{\text{eff}}(\mathbf{k})$ term is the Rashba-Floquet altermagnet Hamiltonian in Eq. (10). The long-range behavior of the exchange interactions is governed by the poles and branch cuts of the Green’s function near the Fermi surface. Because the Floquet-renormalized quasiparticle spectrum determines these singularities, the resulting exchange coupling directly reflects the spin-split and anisotropic structure of the Rashba–alternating magnetic Fermi surface.

In Rashba altermagnets, the matrix structure of Green’s function in spin space is due to the combined presence of RSOC and altermagnetic order, which break inversion and spin-rotation symmetries. As a result, all components of the exchange tensor $J_{\alpha\beta}(\mathbf{R})$ are, in general, finite. Writing the interaction explicitly, the RKKY Hamiltonian reads

$$H_{\text{RKKY}} = J_{xx} S_1^x S_2^x + J_{yy} S_1^y S_2^y + J_{zz} S_1^z S_2^z + J_{xy} (S_1^x S_2^y + S_1^y S_2^x) + J_{xz} (S_1^x S_2^z + S_1^z S_2^x) + J_{yz} (S_1^y S_2^z + S_1^z S_2^y) + \mathbf{D}(\mathbf{R}) \cdot (\mathbf{S}_1 \times \mathbf{S}_2), \quad (17)$$

where the Dzyaloshinskii–Moriya (DM) vector is given by $\mathbf{D} = (J_{yz} - J_{zy}, J_{zx} - J_{xz}, J_{xy} - J_{yx})$. The diagonal terms J_{xx} , J_{yy} , and J_{zz} describe anisotropic Heisenberg exchange interactions. Their anisotropy reflects the momentum-dependent spin polarization of the Rashba-split altermagnetic bands and leads to direction-dependent oscillation periods and decay lengths of the RKKY interaction. Unlike conventional metals, where rotational symmetry enforces isotropic exchange, Rashba altermagnets generically exhibit $J_{xx} \neq J_{yy} \neq J_{zz}$. The symmetric off-diagonal terms J_{xy} , J_{xz} , and J_{yz} arise from spin–orbit–induced spin mixing in the electronic Green’s functions. These terms vanish in centrosymmetric or spin-rotation-invariant systems but are intrinsic to Rashba altermagnets. They encode couplings between orthogonal spin components of the impurities and favor noncollinear magnetic configurations.

The antisymmetric part of the exchange tensor generates the DM interaction, which is permitted by the absence of inversion symmetry. Using $G(\mathbf{R}, E) = G_0(\mathbf{R}, E)\sigma_0 + \mathbf{G}(\mathbf{R}, E) \cdot \boldsymbol{\sigma}$, the exchange interactions are given by

$$\frac{J_{\alpha\alpha}(\mathbf{R})}{J_{\text{sd}}^2} = -\frac{2}{\pi} \text{Im} \int_{-\infty}^{\mu} dE \left(G_0(\mathbf{R}, E)G_0(-\mathbf{R}, E) + G_{\alpha}(\mathbf{R}, E)G_{\alpha}(-\mathbf{R}, E) - \sum_{\beta \neq \alpha} G_{\beta}(\mathbf{R}, E)G_{\beta}(-\mathbf{R}, E) \right), \quad (18a)$$

$$\begin{aligned} \frac{J_{\alpha\beta}(\mathbf{R})}{J_{\text{sd}}^2} = & -\frac{2}{\pi} \text{Im} \int_{-\infty}^{\mu} dE \left(G_{\alpha}(\mathbf{R}, E)G_{\beta}(-\mathbf{R}, E) + G_{\beta}(\mathbf{R}, E)G_{\alpha}(-\mathbf{R}, E) + i \sum_{\xi} \varepsilon_{\alpha\beta\xi} [G_0(\mathbf{R}, E)G_{\xi}(-\mathbf{R}, E) \right. \\ & \left. - G_{\xi}(\mathbf{R}, E)G_0(-\mathbf{R}, E)] \right), \end{aligned} \quad (18b)$$

$$\frac{D_{\alpha}(\mathbf{R})}{J_{\text{sd}}^2} = -\frac{4}{\pi} \text{Im} \int_{-\infty}^{\mu} dE i \left(G_0(\mathbf{R}, E)G_{\alpha}(-\mathbf{R}, E) - G_{\alpha}(\mathbf{R}, E)G_0(-\mathbf{R}, E) \right). \quad (18c)$$

Although Eqs. (18) formally define the full tensorial RKKY interaction, closed analytical expressions are generally unattainable for the effective Hamiltonian in Eq. (10). The Floquet-driven Rashba alter-magnet hosts several competing energy scales, which together produce an anisotropic band structure lacking continuous rotational symmetry. Thus, the real-space Green's functions involve 2D momentum integrals over nonseparable dispersions, rendering standard analytical treatments impractical beyond limiting cases. We therefore compute the Green's functions numerically by discretizing the Brillouin zone on a dense 1000×1000 \mathbf{k} -grid and performing the momentum and energy integrations up to the Fermi level at zero temperature. Because the relevant physics is governed by low-energy states near the Fermi level and the drive frequency exceeds the electronic bandwidth, any non-periodicity at the Brillouin-zone boundaries does not affect the results, implying that Brillouin-zone edge states lie far from the low-energy window.

The diagonal exchange couplings are decomposed into an isotropic Heisenberg component, denoted as $J_{\text{H}} = (J_{xx} + J_{yy} + J_{zz})/3$ and a uniaxial Ising anisotropy $J_{\text{I}} = J_{zz} - (J_{xx} + J_{yy})/2$. This parametrization simplifies the presentation and interpretation of the RKKY results below. The antisymmetric exchange is captured by the DM vector $\mathbf{D}(\mathbf{R})$, whose magnitude sets the strength of the chiral coupling and whose orientation is dictated by RSOC and Floquet-induced symmetry breaking. The sign of each exchange term determines the preferred magnetic alignment of the impurities, while the magnitude controls the interaction strength. A positive (negative) Heisenberg coupling favors anti-ferromagnetic (AFM) or ferromagnetic (FM) alignment. The Ising term enforces collinear order along a selected axis, with its sign determining easy-axis behavior here. The antisymmetric DM interaction sets the chirality of noncollinear textures, selecting clockwise (CW) or counterclockwise (CCW) canting. In a nutshell, magnitudes determine interaction strength, while signs fix the magnetic ground state.

4 Results and discussion

Although the Fermi surface in the present model is anisotropic and band dependent, the electronic states relevant for the RKKY interaction are characterized by a typical momentum scale set by the Fermi momentum k_{F} . We therefore measure all momenta in units of $k_{\text{F}} = 1$, without loss of generality. The dimensionless parameter $\mathcal{A} = eA_0/\hbar k_{\text{F}}$ then directly quantifies the light-induced momentum shift relative to the Fermi surface due to the first beam, while $\mathcal{S}\mathcal{A}$ denotes the corresponding shift induced by the second beam. In dilute or low-carrier-density regimes, k_{F} is substantially reduced compared to conventional metals; for typical 2D densities 10^{10} – 10^{12} cm^{-2} one finds $k_{\text{F}} \sim 10^7$ – 10^8 m^{-1} . Requiring $eA_0/\hbar \sim k_{\text{F}}$ then corresponds to electric-field strengths $E_0 = \omega A_0 \sim 10^7$ – 10^8 V/m for our representative driving frequency $\hbar\omega \geq 1$ eV, which aligns perfectly with visible-light fields, making these nonequilibrium phenomena accessible with standard optical setups. These values are well within the range of standard ultrafast optical experiments [90–94] and lie far below strong-field or breakdown thresholds.

We also note that, because the continuum quadratic dispersion lacks particle–hole symmetry and the Floquet drive induces a scalar Stark shift, the chemical potential $\mu = 0$ considered throughout this manuscript (unless stated otherwise) does not correspond to half filling. Instead, the carrier density is controlled by the Fermi energy measured relative to the light-renormalized band minimum.

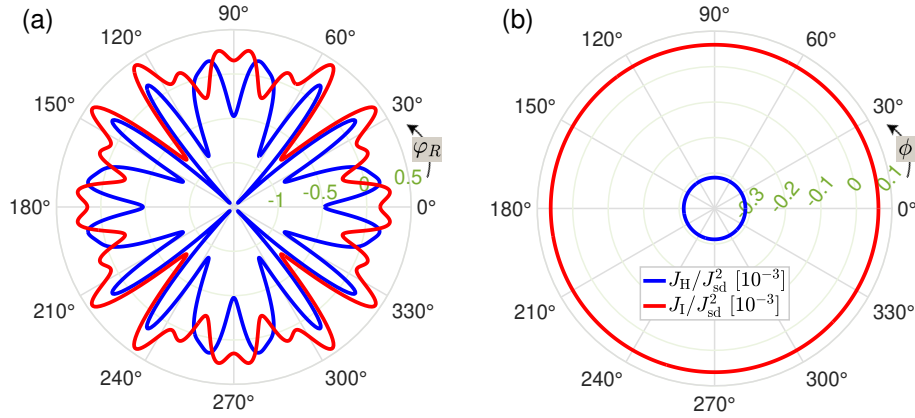


Figure 2: Angular dependence of the RKKY interaction in a 2D Rashba altermagnet for fixed impurity separation $R = 35 \text{ \AA}$, Rashba coupling $\lambda_R = 0.3 \text{ eV}\cdot\text{\AA}$, altermagnetic strength $M_d = 0.7$, and orientation $\theta_M^d = 0$. (a) representative pristine Heisenberg (J_H) and Ising (J_I) components as functions of the relative impurity angle φ_R in the absence of driving, illustrating the 2π periodicity and the intrinsic anisotropy of the altermagnetic band structure. (b) Dependence of the same components on the relative angle ϕ between the two circularly polarized driving fields, showing an essentially isotropic response.

While we present the RKKY results primarily for the $d_{x^2-y^2}$ -wave altermagnet, the efficient optical control discussed below is not symmetry-specific. As demonstrated explicitly in the following band-structure analysis, the same mechanism operates in the d_{xy} -wave altermagnet, indicating that the results are generic across d -wave altermagnetic symmetries.

The RKKY interaction is periodic in the relative impurity orientation,

$$H_{\text{RKKY}}(\varphi_R + 2\pi) = H_{\text{RKKY}}(\varphi_R), \quad (19)$$

as illustrated in Fig. 2(a) for representative Heisenberg (J_H) and Ising (J_I) couplings in a pristine 2D Rashba altermagnet in the absence of driving. Since the driving fields do not couple directly to φ_R , varying this angle does not introduce qualitatively new Floquet-induced exchange mechanisms, but merely rescales the relative weights of existing components. We therefore fix $\varphi_R = \pi/3$ in the following.

Furthermore, although the effective Rashba-Floquet Hamiltonian depends explicitly on the relative phase ϕ of the two laser fields through the in-plane Zeeman-like terms $\Omega_{x,y}$, the resulting static RKKY interaction is insensitive to ϕ , as shown in Fig. 2(b). Thus, varying the relative light angle does not introduce additional anisotropy, but instead leaves the symmetry of the Floquet-engineered exchange interactions intact. This follows from the inversion relation $G_\alpha(\mathbf{R}, E) = G_\alpha^*(-\mathbf{R}, E)$ [Eq. (18)]. Phase-dependent contributions enter with opposite signs at \mathbf{R} and $-\mathbf{R}$, reflecting the inversion relation $G_\alpha(\mathbf{R}, E) = G_\alpha^*(-\mathbf{R}, E)$. As a result, all ϕ -dependent terms appear in antisymmetric combinations that cancel when taking the imaginary part of the exchange integrals, which involve traces over products of Green's functions. We therefore fix $\phi = \pi/3$ throughout. Phase sensitivity may re-emerge for non-collinear impurities or in the presence of dynamical exchange, where the $\mathbf{R} \leftrightarrow -\mathbf{R}$ symmetry and the advanced-retarded cancellation no longer hold; these effects are beyond the scope of the present work. The difference in the radii of two RKKY components reflects distinct Floquet renormalizations of the corresponding exchange channels.

Figure 3 directly compares monochromatic and bichromatic Floquet control of the RKKY interaction in the $d_{x^2-y^2}$ -wave Rashba altermagnet. Under single-color driving [Figs. 3(a)–(e)], all exchange channels are suppressed only once the drive amplitude exceeds a critical value $\mathcal{A}_c \simeq 0.33$ (see the videos in the Supplemental Material (SM) [95]). In contrast, bichromatic driving [Figs. 3(f)–(j)] achieves an equivalent suppression using two weaker beams, with the primary amplitude fixed at $\mathcal{A} = 0.15$, corresponding to a 54% reduction to \mathcal{A}_c , and the second beam providing $\mathcal{S}\mathcal{A} = 0.3$, corresponding to $\simeq 10\%$ reduction to \mathcal{A}_c . To quantify the practical advantage of bichromatic driving, we define the total dimensionless drive strength $\mathcal{A}_{\text{tot}} = \mathcal{A}\sqrt{1 + \mathcal{S}}$, proportional to the total injected optical power. As noted

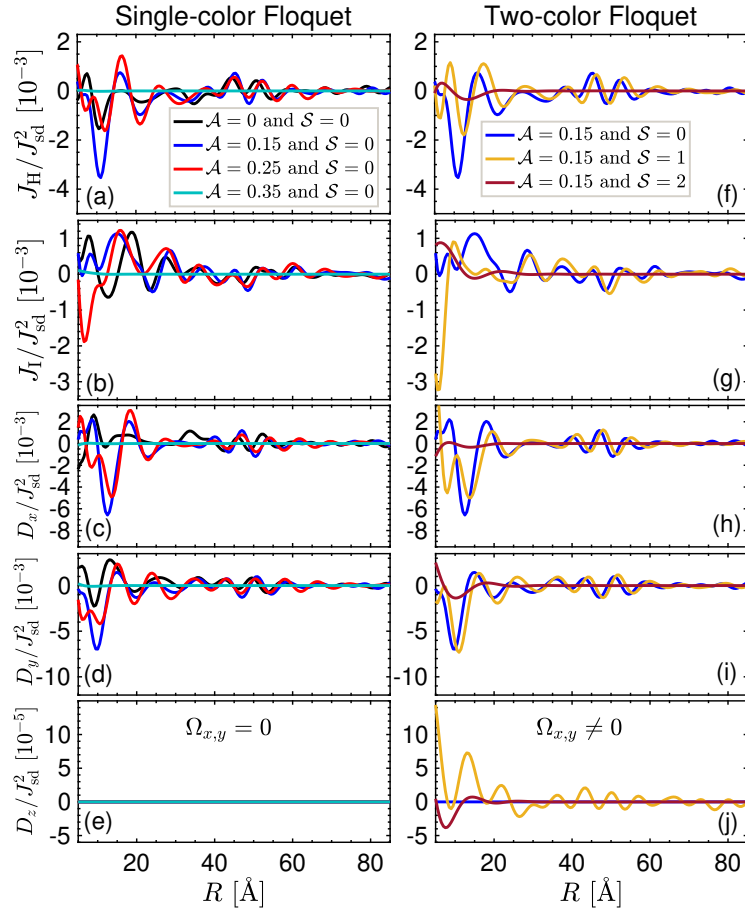


Figure 3: Distance dependence of the Heisenberg (J_H), Ising (J_I), and DM (D_α) components of the RKKY interaction under single- and two-color driving for fixed Rashba coupling $\lambda_R = 0.3 \text{ eV}\cdot\text{\AA}$, alternating strength $M_d = 0.7$, and orientation $\theta_M^d = 0$. While single-color driving [(a)–(e)] suppresses all exchange channels only at large amplitudes, two-color driving achieves comparable suppression at substantially reduced peak fields [(f)–(j)] with a 54% reduction in the primary beam amplitude and the addition of a secondary beam whose amplitude is also reduced by 10%, demonstrating a markedly more efficient control protocol.

above, in the monochromatic case, switching occurs at a critical amplitude $\mathcal{A}_c \simeq 0.33$, corresponding to a total amplitude $\mathcal{A}_{\text{tot}} = \mathcal{A}_c$. In contrast, the same total drive strength can be realized in the bichromatic scheme using two substantially weaker beams, e.g., $(\mathcal{A}, S\mathcal{A}) = (0.15, 0.3)$, $(\mathcal{A}, S\mathcal{A}) = (0.175, 0.28)$, or $(\mathcal{A}, S\mathcal{A}) = (0.2, 0.26)$, with both amplitudes well below the single-color threshold. Although the total injected optical power is comparable in both protocols, the peak power of each individual beam is substantially reduced in the bichromatic scheme, which is advantageous for minimizing heating, nonlinear absorption, and breakdown of the high-frequency Floquet regime.

Under both driving protocols, the magnetic impurities exhibit separation-dependent FM/AFM and CW/CCW alignments, reflecting sign changes that evolve with the light intensity. While single-color driving suppresses the RKKY interaction in a largely monotonic fashion, at short distances, bichromatic driving induces a pronounced reshaping of the oscillatory structure of the exchange interaction. This behavior reflects interference between photon sectors, which modifies the real-space Green's functions and selectively suppresses Fermi-surface contributions while leaving short-distance, high-momentum processes partially intact. This effect arises from Floquet-induced in-plane Zeeman-like fields $\Omega_{x,y}$ generated by two-color driving, as noted in Tab. 1, which preferentially modify high-momentum states that dominate the short-range exchange.

A key qualitative distinction between the two driving protocols, Figs. 3(e) and 3(f), is the emergence

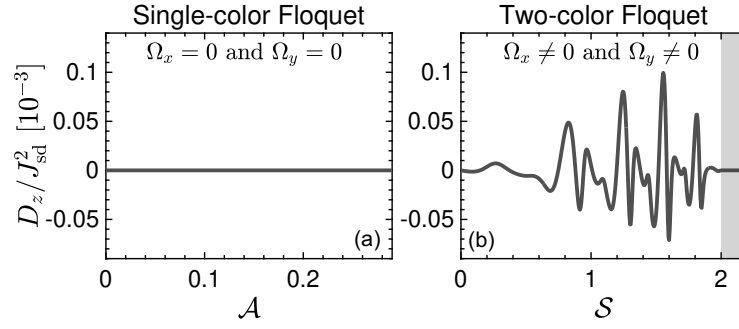


Figure 4: Out-of-plane DM interaction D_z as a function of the drive parameter (a) \mathcal{A} and (b) \mathcal{S} under single- and two-color driving, respectively, at fixed impurity separation $R = 35 \text{ \AA}$, Rashba coupling $\lambda_R = 0.3 \text{ eV}\cdot\text{\AA}$, altermagnetic strength $M_d = 0.7$, and altermagnetic orientation $\theta_M^d = 0$. While D_z is strictly forbidden under monochromatic circular driving, bichromatic excitation induces a sizable and oscillatory D_z due to Floquet-engineered in-plane Zeeman-like fields Ω_x and Ω_y in Eq. (10).

of a finite out-of-plane DM interaction D_z under bichromatic excitation, as also shown in Fig. 4. This component is symmetry-forbidden in equilibrium and under single-color driving, and cannot be activated by simply increasing the drive amplitude \mathcal{A} [Fig. 4(a)]. Microscopically, the in-plane Zeeman-like terms $\Omega_{x,y}$ generated by two-color interference enhance antisymmetric spin mixing in the real-space Green's functions, directly producing a finite D_z as a genuine dynamical Floquet effect. Moreover, D_z vanishes permanently for $\mathcal{S} \gtrsim \mathcal{S}_c \simeq 2$ (corresponding to $\mathcal{S}_c \mathcal{A} \approx 0.3$) [Fig. 4(b)], as discussed below.

Practically, a finite out-of-plane component of the DM interaction, D_z , favors in-plane cycloidal or helical spin spirals and is essential for stabilizing in-plane chiral textures such as Néel-type domain walls, planar spin spirals, and chiral edge states in 2D magnets [96–102]. In equilibrium Rashba altermagnets, as well as under single-color driving, crystalline symmetries typically forbid a finite D_z , rendering these textures unstable or symmetry-forbidden. By contrast, within the Floquet framework, two-color laser driving dynamically breaks the relevant symmetries and induces a finite D_z , thereby enlarging the magnetic phase space and enabling in-plane chiral states inaccessible under equilibrium or single-color conditions. Moreover, D_z enables robust information encoding and low-energy manipulation in racetrack and spintronic devices.

The suppression of the RKKY interaction, beyond the critical values $\mathcal{A}_c \simeq 0.33$ and $\mathcal{S}_c \simeq 2$ for both the single- and two-color schemes, is directly linked to the Floquet-modified band structure. The strength, sign, and anisotropy of the RKKY coupling are determined by the dispersion, spin texture, and density of states near the Fermi level. Accordingly, in Fig. 5, we focus on the lower Floquet band dispersion of the effective Hamiltonian in Eq. (10) for different parameters. Red lines in Fig. 5 indicate the states available at the Fermi surface. Starting from a conventional 2D electron gas [Fig. 5(a)] with $M_d = \lambda_R = \mathcal{A} = \mathcal{S} = 0$, the dispersion is purely parabolic and touches the chemical potential at $\mathbf{k} = 0$, yielding a negligible density of states and RKKY interactions. Introducing RSOC [Fig. 5(b)] lowers the band minimum and generates finite Fermi-level states, while a strong altermagnetic order [Fig. 5(c)] renders the dispersion anisotropic with momentum-dependent spin splitting, thereby shaping the symmetry and anisotropy of the RKKY interaction.

Under single-color circular driving [Fig. 5(d)], Floquet hybridization alters the low-energy bands through virtual photon processes, but moving the band minimum past μ demands either large field amplitudes near the high-frequency limit (see SM [95]) or adjustment of μ . Both approaches are intrinsically fragile: the chemical potential is sensitive to disorder and thermal broadening, while single-color Floquet band shifts require amplitudes approaching the limits of the high-frequency regime. Consequently, on-off switching of the RKKY interaction via μ tuning or large \mathcal{A} is highly parameter-sensitive and difficult to control systematically. For completeness, Fig. 8 illustrates how weak doping influences the switching behavior under both single- and two-color driving. In contrast, bichromatic driving [Figs. 5(e)–(h)] offers an intrinsic and efficient control mechanism: interference between photon sectors coherently shifts the global minimum of the lower Floquet band upward, enabling a controlled Lifshitz-like disappearance of the Fermi surface with just two weak beams. The Lifshitz-like transition occurs when $\min_{\mathbf{k}} E_-(\mathbf{k}, \mathcal{S}_c) = \mu$. Let $\mathbf{k}_0(\mathcal{S})$ denote the momentum minimizing $E_-(\mathbf{k})$,

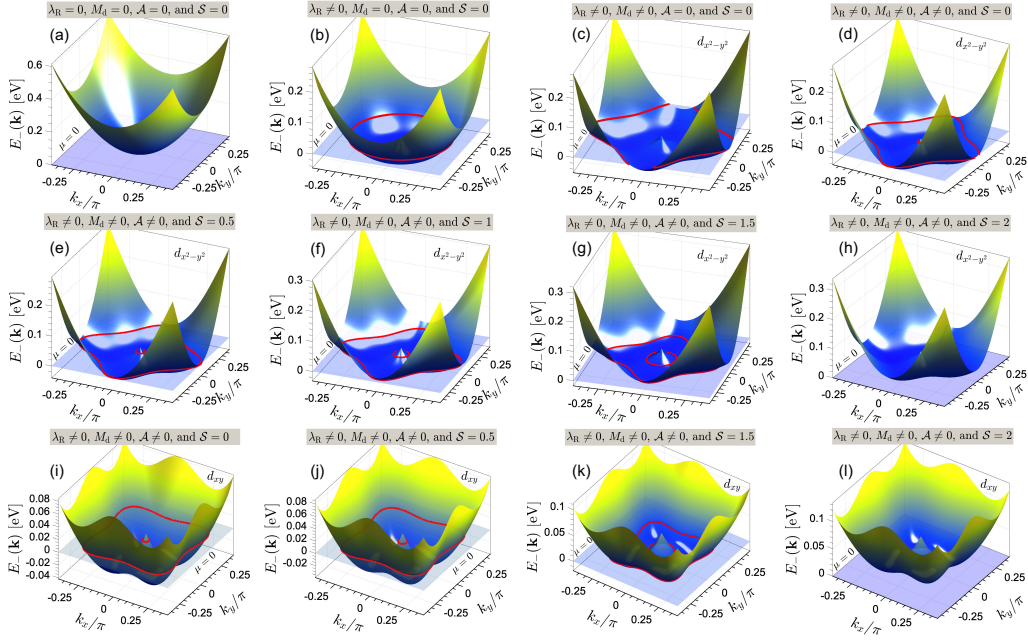


Figure 5: Evolution of the lower Floquet quasienergy band $E_-(\mathbf{k})$ in a 2D Rashba altermagnet under monochromatic and bichromatic driving for $d_{x^2-y^2}$ - and d_{xy} -wave altermagnets. Starting from a (a) parabolic dispersion above the Fermi level ($\mu = 0$) in the absence of RSOC, altermagnetism, and driving, successive tuning of (b) λ_R , (c) M_d , and (d)–(l) the laser parameters reshapes the low-energy electronic structure. Red lines on the $\mu = 0$ plane indicate the corresponding Fermi surfaces. (d) Single-color driving ($\mathcal{A} = 0.15$, $\mathcal{S} = 0$) in the $d_{x^2-y^2}$ -wave altermagnet modifies the band extrema via virtual photon processes, partially tuning states at the Fermi level. In contrast, (e)–(h) bichromatic driving systematically shifts the global minimum of $E_-(\mathbf{k})$ upward with increasing \mathcal{S} , inducing a controlled Lifshitz-like disappearance of the Fermi surface. (i)–(l) The same behavior is observed for the d_{xy} -wave altermagnet, demonstrating that the Floquet-engineered Lifshitz transition is robust across different altermagnetic symmetries. Parameters are $\lambda_R = 0.3 \text{ eV}\cdot\text{\AA}$, $M_d = 0.7$, $\eta_{1,2} = +1$, and $\theta_M^d = 0$ ($\pi/4$) for the $d_{x^2-y^2}$ - (d_{xy} -) wave case.

$\nabla_{\mathbf{k}} E_-(\mathbf{k}, \mathcal{S})|_{\mathbf{k}=\mathbf{k}_0} = 0$. Then \mathcal{S}_c satisfies

$$\varepsilon k_0^2 + \mu_\omega(\mathcal{S}_c) = \mu + \sqrt{|\mathbf{h}(\mathbf{k}_0, \mathcal{S}_c)|^2}. \quad (20)$$

For $\lambda_R = 0.3 \text{ eV}\cdot\text{\AA}$, $M_d = 0.7$, $\theta_M^d = 0$, $\mu = 0$, $\eta_1 = \eta_2 = +1$, $\hbar\omega = 3 \text{ eV}$, and $\mathcal{A} = 0.15$, we find $\mathcal{S}_c \simeq 2$ for the $d_{x^2-y^2}$ -wave altermagnet, consistent with Fig. 3 and SM videos [95]. Thus, this Lifshitz-like disappearance serves as the main mechanism driving the on–off switching of the RKKY interaction.

Importantly, this mechanism is robust across different altermagnetic symmetries. Although the lower band exhibits distinct energy distributions across the Brillouin zone for $d_{x^2-y^2}$ - and d_{xy} -wave altermagnets, see Figs. 5(i)–(l), the critical value \mathcal{S}_c at which the bands are shifted entirely above μ is nearly the same in both cases. Thus, for energies below μ , one expects different oscillatory behaviors of the RKKY interaction, whereas the on–off switching process is essentially identical for the two symmetries. These findings are expected to generalize to other g -, f -, and i -wave forms [62]. The required amplitude of the second laser beam to achieve an upward shift of the lower band may vary with symmetry, but the essential mechanism—a robust and controllable on–off modulation of the RKKY interaction using bichromatic laser driving—remains valid.

We further note that \mathcal{S}_c is robust against weak nonmagnetic disorder that preserves the average crystal symmetry and does not qualitatively alter the band structure. Moderate disorder broadens quasiparticle states but leaves the band minimum unchanged, so the Lifshitz-like disappearance of the

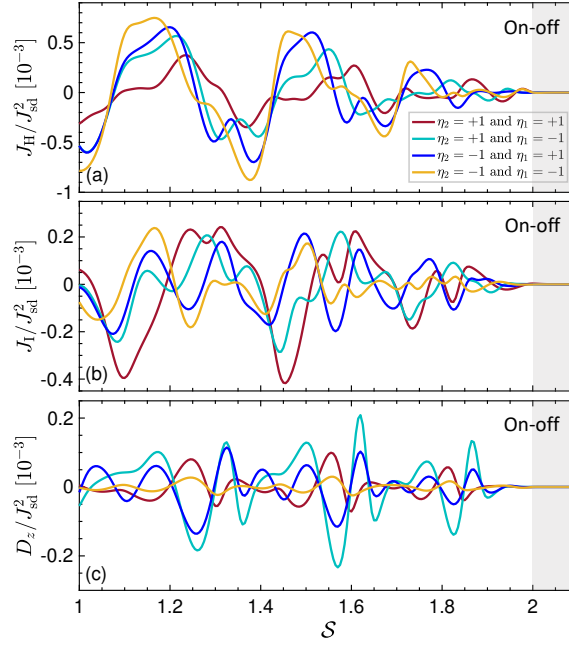


Figure 6: Dependence of the RKKY interaction components, (a) Heisenberg J_H , (b) Ising J_I , and (c) DM D_z on the relative amplitude S of the second laser beam for fixed impurity separation $R = 35 \text{ \AA}$ for equal (opposite) chiralities of the two beams. All configurations exhibit nearly the same critical value of $S_c \simeq 2$ at which the RKKY interaction rapidly vanishes. Parameters are $\lambda_R = 0.3 \text{ eV} \cdot \text{\AA}$, $M_d = 0.7$, $\theta_M^d = 0$, and $\mathcal{A} = 0.15$.

Fermi surface remains well defined as long as the broadening is smaller than the Floquet gap and spin-orbit energy scales. Finite temperature also smooths the Fermi edge, reducing crossover sharpness but not eliminating it, provided $k_B T$ is below the energy separation between the band minimum and the chemical potential near S_c . In this regime, Fermi-surface contributions to the RKKY interaction remain suppressed, while residual exchange via virtual Floquet processes persists. As a result, S_c represents a robust crossover scale rather than a fine-tuned critical point, and the on-off switching mechanism survives under realistic disorder and finite-temperature conditions.

Since D_x and D_y appear in both driving schemes, while D_z is unique to the two-color case, we take D_z as the representative DM component in the following.

Figure 6 shows how bichromatic driving tunes the strength and magnetic alignment of the impurities via the relative beam amplitude S at fixed impurity separation $R = 35 \text{ \AA}$, focusing on various chiralities between the beams. For most S , all exchange channels remain finite, indicating coherent spin mediation at the Fermi level. As S increases, the interactions first show nonmonotonic oscillations, then rapidly suppress at a critical ratio $S_c \simeq 2$ for both equal and opposite chiralities. It is clear that the chirality of the two beams can switch the interaction between FM and AFM in J_H and J_I , as well as toggle the magnetic phase of the two impurities between CW and CCW in D_z . The strong dependence on laser chirality reflects the symmetry-selective nature of bichromatic Floquet engineering, providing an additional control over the magnitude and sign of the RKKY interaction.

Next, Fig. 7 maps the phase diagram (M_d, λ_R) for three two-color amplitude ratios S , delineating regimes with or without available Fermi-level states and the corresponding suppression of the RKKY interaction, together with the resulting FM/AFM and CW/CCW impurity alignments. For weak driving ($S = 0.5$), all components oscillate, reflecting Fermi-level states mediating long-range exchange. Alternating FM/AFM and CW/CCW regions arise from interference between Rashba spin-momentum locking and the altermagnetic field, while sizable D_z appears only under strong altermagnetic order and RSOC in the two-color driving scheme due to broken effective symmetries. At intermediate driving ($S = 1.5$), the regions with finite exchange shrink, with oscillations confined to narrow bands at larger λ_R and M_d , reflecting the Floquet-induced upward shift of the band minimum and depletion of low-energy states. Suppression of all components indicates a common electronic origin tied to Fermi-surface

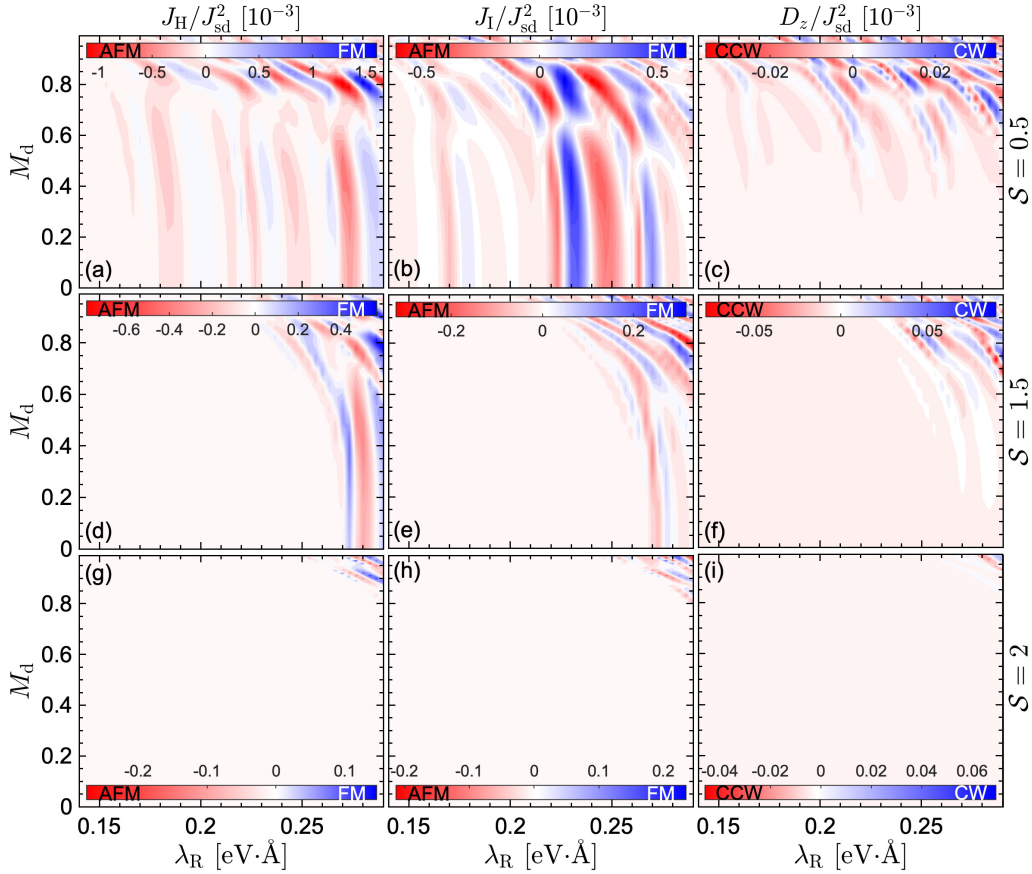


Figure 7: RKKY interaction components as functions of Rashba coupling λ_R and alternating magnetic strength M_d for $R = 35 \text{ \AA}$ and primary light amplitude $\mathcal{A} = 0.15$. Columns (left to right) show Heisenberg J_H , Ising J_I , and out-of-plane DM D_z . Rows (top to bottom) correspond to two-color ratios $S = 0.5, 1.5$, and 2 . Red (blue) indicates AFM (FM) alignment for J_H and J_I , and CCW (CW) chirality for D_z . Increasing S progressively suppresses all components, nearly switching off the RKKY interaction, except for narrow surviving regions at $\lambda_R \gtrsim 0.25 \text{ eV}\cdot\text{\AA}$ in a strong altermagnet.

availability. For strong driving ($S = 2$), the RKKY interaction is nearly extinguished, with residual signals only at extreme parameter edges, confirming robust Floquet-induced switching. The concurrent disappearance of FM/AFM and CW/CCW regions confirms suppression arises from the genuine loss of Fermi-level states rather than channel cancellation.

So far, all results were obtained at charge neutrality ($\mu = 0$). We now examine the effects of dilute hole ($\mu < 0$) and electron ($\mu > 0$) doping, focusing on the representative Heisenberg interaction J_H in Fig. 8. Figure 8 summarizes how the chemical potential μ controls Floquet-driven tuning of the RKKY interaction under single- and two-color driving. At charge neutrality, J_H exhibits oscillations followed by rapid suppression beyond a critical threshold. Oscillations are more regular under \mathcal{A} -driving, while they are sharper under S -driving, highlighting the efficiency of bichromatic interference in reshaping Floquet bands.

Hole doping ($\mu < 0$) accelerates the extinction of J_H , which collapses at much smaller \mathcal{A} and S due to an upward shift of Floquet bands relative to the Fermi level. Electron doping ($\mu > 0$) enhances J_H and extends its range, as Floquet-renormalized conduction-band states continue to mediate long-range exchange. Notably, for $\mu > 0$, single-color driving requires a strong amplitude ($\mathcal{A} \gtrsim 0.5$) to suppress J_H , whereas two-color driving achieves on-off switching at much weaker fields. For example, with $\mathcal{A} = 0.15$, tuning S to $S_c \simeq 2.6$ suffices to shift the lower Floquet bands above the chemical potential and suppress the exchange. This efficiency arises from interference between the two frequencies, which selectively redistributes spectral weight and opens low-energy gaps without large overall amplitudes.

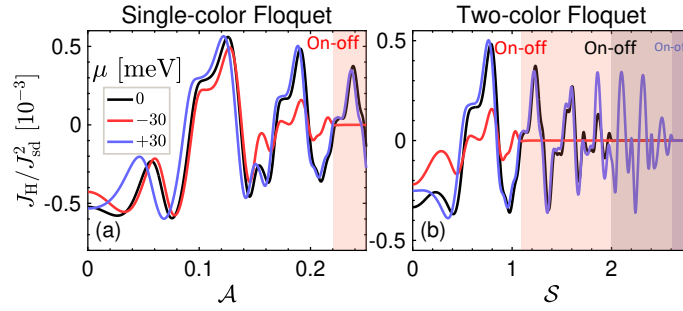


Figure 8: Dependence of the representative Heisenberg RKKY interaction J_H on mono- and bi-chromatic Floquet driving for different chemical potentials μ : hole doping ($\mu < 0$), charge neutrality ($\mu = 0$), and electron doping ($\mu > 0$). (a) Single-color driving: J_H versus drive amplitude \mathcal{A} at $\mathcal{S} = 0$. (b) Two-color driving: J_H versus relative strength \mathcal{S} at $\mathcal{A} = 0.15$. Both protocols allow optical control and eventual suppression of the exchange, but the onset, robustness, and switching threshold are asymmetric in μ : hole doping accelerates suppression, while electron doping enhances J_H and delays switching. Parameters: $\lambda_R = 0.3 \text{ eV}\cdot\text{\AA}$, $M_d = 0.7$, and $R = 35 \text{ \AA}$.

Therefore, even within the same doping protocol, two-color laser driving provides a substantially more efficient and experimentally favorable route to control and switch the RKKY interaction.

5 Experimental relevance and material platforms

Our results are directly relevant to a growing class of 2D systems combining RSOC with altermagnetic order. Promising platforms include altermagnetic thin films and surfaces derived from recently identified bulk altermagnets, as well as engineered heterostructures where altermagnetic layers are interfaced with heavy-element substrates to enhance RSOC. Candidate materials include $\text{KV}_2\text{Se}_2\text{O}$ [103], $\text{RbV}_2\text{Te}_2\text{O}$ [104], $\kappa\text{-CL}$ [7], and RuO_2 [5, 10, 18, 105, 106], though the latter remains debated. The RKKY interaction can be realized experimentally using localized magnetic moments introduced as adatoms or substitutional impurities on the host surface. Such spins can be individually positioned and probed via scanning tunneling microscopy (STM) [107], allowing direct access to the spatial structure and strength of the indirect exchange.

Floquet control and on-off switching of the RKKY interaction can be detected using several complementary probes. In STM setups, laser-induced changes would manifest as modifications of impurity-induced bound states or spin-excitation spectra. At higher impurity densities, switching could appear indirectly through altered magnetic ordering or correlation lengths. Time-resolved pump-probe techniques further allow direct tracking of nonequilibrium exchange dynamics via transient spin responses following bichromatic excitation [63–72]. A concrete realization would then involve ω – 2ω bicircular pumping combined with STM-based impurity spectroscopy on altermagnetic thin films.

6 Summary and outlook

In real experimental setups, magnetic impurities can mask the intrinsic spin-dependent properties of the host material. Moreover, because these impurities interact indirectly through the RKKY mechanism, the performance of applications based on single-spin impurities is inherently limited. This highlights the need for an efficient control knob that can both reveal the pristine electronic and spin features of the host and enable practical single-impurity applications. Such a control scheme should be capable of suppressing the RKKY interaction as much as possible, allowing the intrinsic host information to be extracted while effectively decoupling impurity spins for qubit, sensing, or spintronic applications.

In this work, we have shown that bichromatic laser driving enables efficient, symmetry-selective control of the RKKY interaction in Rashba altermagnets. Our analysis is based on a high-frequency

Floquet expansion and assumes weak impurity–electron coupling, such that the RKKY interaction is well described by second-order perturbation theory. By deriving the effective Floquet Hamiltonian and computing real-space Green’s functions, we showed that the interplay between altermagnetic order and light-induced spin–orbit renormalization drives a controllable, Lifshitz-like disappearance of the Fermi surface, allowing robust on–off switching of indirect magnetic exchange at substantially reduced peak field strengths compared to monochromatic driving. The observed transition differs from an equilibrium Lifshitz transition driven by changes in band topology or carrier density. Instead, it corresponds to a Floquet-induced band-edge crossing controlled dynamically by external fields, without altering the underlying lattice symmetry or requiring fine-tuning of the chemical potential.

This mechanism is insensitive to impurity orientation and altermagnetic symmetry, and naturally generates exchange channels, such as an out-of-plane DM interaction, that are forbidden in equilibrium or under single-color illumination. Notably, the resulting RKKY interaction is also insensitive to the relative phase of the two driving fields, reflecting a cancellation of phase-dependent contributions arising from the combined role of Green’s functions at \mathbf{R} and $-\mathbf{R}$ in the exchange integrals.

Our analysis further establishes altermagnetism as a key ingredient for realizing nontrivial and controllable RKKY textures under two-color driving. In the absence of altermagnetic order, the Green’s function remains diagonal in spin space, leading only to conventional, collinear exchange interactions similar to those in massive 2D Rashba electron gases. By contrast, finite altermagnetic order generates in-plane spin–orbit fields and anisotropic exchange channels, which are directly responsible for the enhanced tunability and robustness of the laser-controlled switching. Our results establish bichromatic Floquet engineering as a versatile route for dynamically controlling long-range magnetic interactions in low-dimensional quantum materials.

The results presented here open several avenues for future theoretical and experimental research. The bichromatic Floquet framework can be extended to other magnetic platforms where indirect exchange is important, including antiferromagnets, ferrimagnets, and noncollinear metals. In particular, applying two-color driving to systems with Dirac or multi-valley band structures could enable valley- or sublattice-selective RKKY switching, providing additional control beyond altermagnets. While moderate disorder and finite temperature are not expected to qualitatively alter the Floquet-induced band shifts, strong scattering or low-frequency driving may invalidate the effective Hamiltonian description. Exploring these regimes remains an interesting direction for future work.

Author contributions M. Y. and J. K. F. conceived the project, supervised the research, contributed to the interpretation of the results, and assisted in writing the final manuscript. M. Y. and P.-H. F. performed the preliminary analytical calculations. M. Y. carried out all numerical calculations, prepared the figures, and drafted the manuscript. All authors discussed the results, contributed to the writing of the manuscript, and approved the final version.

Funding information M. Y. and J. K. F. were supported by the Department of Energy, Office of Basic Energy Sciences, Division of Materials Sciences and Engineering under Contract No. DE-FG02-08ER46542 for the formal developments, the numerical work, and the writing of the manuscript. J. F. K. was also supported by the McDevitt bequest at Georgetown University. P.-H. F. acknowledges the financial support from the Fondazione Cariplo under the grant 2023-2594 for preliminary analytical calculations and discussion. M. Y. and P.-H. F. thank S. A. A. Ghorashi for useful discussions.

References

- [1] L. Šmejkal, J. Sinova and T. Jungwirth, *Emerging research landscape of altermagnetism*, Phys. Rev. X **12**, 040501 (2022), doi:[10.1103/PhysRevX.12.040501](https://doi.org/10.1103/PhysRevX.12.040501).
- [2] L. Šmejkal, J. Sinova and T. Jungwirth, *Beyond conventional ferromagnetism and anti-ferromagnetism: A phase with nonrelativistic spin and crystal rotation symmetry*, Phys. Rev. X **12**, 031042 (2022), doi:[10.1103/PhysRevX.12.031042](https://doi.org/10.1103/PhysRevX.12.031042).

- [3] I. Mazin, *Editorial: Altermagnetism—a new punch line of fundamental magnetism*, Phys. Rev. X **12**, 040002 (2022), doi:[10.1103/PhysRevX.12.040002](https://doi.org/10.1103/PhysRevX.12.040002).
- [4] J. Krempaský, L. Šmejkal, S. W. D'Souza, M. Hajlaoui, G. Springholz, K. Uhlířová, F. Alarab, P. C. Constantinou, V. Strocov, D. Usanov *et al.*, *Altermagnetic lifting of Kramers spin degeneracy*, Nature **626**(7999), 517 (2024), doi:[10.1038/s41586-023-06907-7](https://doi.org/10.1038/s41586-023-06907-7).
- [5] L. Šmejkal, R. González-Hernández, T. Jungwirth and J. Sinova, *Crystal time-reversal symmetry breaking and spontaneous Hall effect in collinear antiferromagnets*, Science Advances **6**(23), eaaz8809 (2020), doi:[10.1126/sciadv.aaz8809](https://doi.org/10.1126/sciadv.aaz8809).
- [6] K.-H. Ahn, A. Hariki, K.-W. Lee and J. Kuneš, *Antiferromagnetism in RuO₂ as d-wave pomeranchuk instability*, Phys. Rev. B **99**, 184432 (2019), doi:[10.1103/PhysRevB.99.184432](https://doi.org/10.1103/PhysRevB.99.184432).
- [7] M. Naka, S. Hayami, H. Kusunose, Y. Yanagi, Y. Motome and H. Seo, *Spin current generation in organic antiferromagnets*, Nature Communications **10**(1), 4305 (2019), doi:[10.1038/s41467-019-12229-y](https://doi.org/10.1038/s41467-019-12229-y).
- [8] S. Hayami, Y. Yanagi and H. Kusunose, *Momentum-dependent spin splitting by collinear antiferromagnetic ordering*, Journal of the Physical Society of Japan **88**(12), 123702 (2019), doi:[10.7566/JPSJ.88.123702](https://doi.org/10.7566/JPSJ.88.123702).
- [9] L. Šmejkal, A. B. Hellenes, R. González-Hernández, J. Sinova and T. Jungwirth, *Giant and tunneling magnetoresistance in unconventional collinear antiferromagnets with nonrelativistic spin-momentum coupling*, Phys. Rev. X **12**, 011028 (2022), doi:[10.1103/PhysRevX.12.011028](https://doi.org/10.1103/PhysRevX.12.011028).
- [10] H. Bai, L. Han, X. Y. Feng, Y. J. Zhou, R. X. Su, Q. Wang, L. Y. Liao, W. X. Zhu, X. Z. Chen, F. Pan, X. L. Fan and C. Song, *Observation of spin splitting torque in a collinear antiferromagnet RuO₂*, Phys. Rev. Lett. **128**, 197202 (2022), doi:[10.1103/PhysRevLett.128.197202](https://doi.org/10.1103/PhysRevLett.128.197202).
- [11] H. Bai, Y. C. Zhang, Y. J. Zhou, P. Chen, C. H. Wan, L. Han, W. X. Zhu, S. X. Liang, Y. C. Su, X. F. Han, F. Pan and C. Song, *Efficient spin-to-charge conversion via altermagnetic spin splitting effect in antiferromagnet RuO₂*, Phys. Rev. Lett. **130**, 216701 (2023), doi:[10.1103/PhysRevLett.130.216701](https://doi.org/10.1103/PhysRevLett.130.216701).
- [12] T. Jungwirth, R. M. Fernandes, J. Sinova and L. Smejkal, *Altermagnets and beyond: Nodal magnetically-ordered phases*, arXiv:2409.10034 (2024), doi:[10.48550/arXiv.2409.10034](https://doi.org/10.48550/arXiv.2409.10034).
- [13] L. Bai, W. Feng, S. Liu, L. Šmejkal, Y. Mokrousov and Y. Yao, *Altermagnetism: Exploring new frontiers in magnetism and spintronics*, Adv. Funct. Mater. **34**(2409327) (2024), doi:[10.1002/adfm.202409327](https://doi.org/10.1002/adfm.202409327).
- [14] T. Jungwirth, R. M. Fernandes, E. Fradkin, A. H. MacDonald, J. Sinova and L. Smejkal, *Altermagnetism: an unconventional spin-ordered phase of matter*, arXiv:2411.00717 (2025), doi:[10.48550/arXiv.2411.00717](https://doi.org/10.48550/arXiv.2411.00717).
- [15] Y. Fukaya, B. Lu, K. Yada, Y. Tanaka and J. Cayao, *Superconducting phenomena in systems with unconventional magnets*, J. Phys.: Condens. Matter **37**, 313003 (2025), doi:[10.1088/1361-648X/adf1cf](https://doi.org/10.1088/1361-648X/adf1cf).

- [16] A. Bose, N. J. Schreiber, R. Jain, D.-F. Shao, H. P. Nair, J. Sun, X. S. Zhang, D. A. Muller, E. Y. Tsymbal, D. G. Schlom and D. C. Ralph, *Tilted spin current generated by the collinear antiferromagnet ruthenium dioxide*, Nature Electronics **5**(5), 267 (2022), doi:[10.1038/s41928-022-00744-8](https://doi.org/10.1038/s41928-022-00744-8).
- [17] L. Han, X. Fu, R. Peng, X. Cheng, J. Dai, L. Liu, Y. Li, Y. Zhang, W. Zhu, H. Bai, Y. Zhou, S. Liang *et al.*, *Electrical 180° switching of Néel vector in spin-splitting antiferromagnet*, Science Advances **10**(4), eadn0479 (2024), doi:[10.1126/sciadv.adn0479](https://doi.org/10.1126/sciadv.adn0479).
- [18] Z. Feng, X. Zhou, L. Šmejkal, L. Wu, Z. Zhu, H. Guo, R. González-Hernández, X. Wang, H. Yan, P. Qin, X. Zhang, H. Wu *et al.*, *An anomalous Hall effect in altermagnetic ruthenium dioxide*, Nature Electronics **5**(11), 735 (2022), doi:[10.1038/s41928-022-00866-z](https://doi.org/10.1038/s41928-022-00866-z).
- [19] Y. Fang, J. Cano and S. A. A. Ghorashi, *Quantum geometry induced non-linear transport in altermagnets*, Phys. Rev. Lett. **133**, 106701 (2024), doi:[10.1103/PhysRevLett.133.106701](https://doi.org/10.1103/PhysRevLett.133.106701).
- [20] H. Yan, X. Zhou, P. Qin and Z. Liu, *Review on spin-split antiferromagnetic spintronics*, Applied Physics Letters **124**(3) (2024), doi:[10.1063/5.0184580](https://doi.org/10.1063/5.0184580).
- [21] P. Fu, Q. Lv, Y. Xu, J. Cayao, J. Liu and X. Yu, *All-electrically controlled spintronics in altermagnetic heterostructures*, npj Quantum Mater. **10**, 111 (2025), doi:[10.1038/s41535-025-00827-7](https://doi.org/10.1038/s41535-025-00827-7).
- [22] A. Herasymchuk, K. B. Hallberg, E. W. Hodt, J. Linder, E. V. Gorbar and P. Sukhachov, *Electric and spin current vortices in altermagnets*, Phys. Rev. B **112**, L220404 (2025), doi:[10.1103/3sw6-y8vf](https://doi.org/10.1103/3sw6-y8vf).
- [23] Z. Zhu, X. Chen, X. Duan, Z. Cui, J. Zhang, I. Žutić and T. Zhou, *Altermagnetolectric spin field effect transistor*, arXiv:2512.02974 (2025).
- [24] T. Kokkeler, T. T. Heikkilä and F. S. Bergeret, *Nonequilibrium spin-splitter effect in altermagnet superconductor hybrids*, arXiv:2510.11355 (2025).
- [25] X. Yang, S. Fang, Z. Yang, P. Ho, J. Lu and Y. S. Ang, *Altermagnetic flatband-driven Fermi surface geometry for giant tunneling magnetoresistance*, arXiv:2511.17277 (2025).
- [26] Z. Yang, X. Yang, J. Wang, Q. Li, R. Peng, C. H. Lee, L. K. Ang, J. Lu, Y. S. Ang and S. Fang, *Unconventional thickness scaling of coherent tunnel magnetoresistance in altermagnets*, Phys. Rev. B **112**, 205202 (2025), doi:[10.1103/2thy-fzzj](https://doi.org/10.1103/2thy-fzzj).
- [27] S. Fang, Z. Yang, J. Wang, X. Yang, J. Lu, C. H. Lee, X. Wang and Y. S. Ang, *Edgetronics in two-dimensional altermagnets*, arXiv:2508.10451 (2025).
- [28] R. Peng, S. Fang, P. Ho, F. Liu, T. Zhou, J. Liu and Y. S. Ang, *Ferroelastic altermagnetism*, npj Quantum Mater. (2025), doi:[10.1038/s41535-025-00835-7](https://doi.org/10.1038/s41535-025-00835-7).
- [29] E. Schwartz, H. Vakili and A. A. Kovalev, *Theory of thermomagnonic torques in altermagnets*, arXiv:2512.14660 (2025).
- [30] H. Yoshida, J. Priessnitz, L. Šmejkal and S. Murakami, *Quantization of spin circular photogalvanic effect in altermagnetic Weyl semimetals*, arXiv:2509.05620 (2025).
- [31] L. E. Golub, *Edge spin galvanic effect in altermagnets*, arXiv:2512.04798 (2025).

- [32] V. Sunko and J. Orenstein, *Linear magneto-birefringence as a probe of altermagnetism*, arXiv:2511.16421 (2025).
- [33] I. V. Maznichenko, A. Ernst, D. Maryenko, V. K. Dugaev, E. Y. Sherman, P. Buczek, S. S. P. Parkin and S. Ostanin, *Fragile altermagnetism and orbital disorder in mott insulator LaTiO_3* , Phys. Rev. Materials **8**(6), 064403 (2024), doi:[10.1103/PhysRevMaterials.8.064403](https://doi.org/10.1103/PhysRevMaterials.8.064403).
- [34] S. Karube, T. Tanaka, D. Sugawara, N. Kadoguchi, M. Kohda and J. Nitta, *Observation of spin-splitter torque in collinear antiferromagnetic RuO_2* , Phys. Rev. Lett. **129**, 137201 (2022), doi:[10.1103/PhysRevLett.129.137201](https://doi.org/10.1103/PhysRevLett.129.137201).
- [35] X. Duan, J. Zhang, Z. Zhu, Y. Liu, Z. Zhang, I. Žutić and T. Zhou, *Antiferroelectric altermagnets: Antiferroelectricity alters magnets*, Phys. Rev. Lett. **134**, 106801 (2025), doi:[10.1103/PhysRevLett.134.106801](https://doi.org/10.1103/PhysRevLett.134.106801).
- [36] M. Gu, Y. Liu, H. Zhu, K. Yananose, X. Chen, Y. Hu, A. Stroppa and Q. Liu, *Ferroelectric switchable altermagnetism*, Phys. Rev. Lett. **134**, 106802 (2025), doi:[10.1103/PhysRevLett.134.106802](https://doi.org/10.1103/PhysRevLett.134.106802).
- [37] P. Werner, M. Lysne and Y. Murakami, *High harmonic generation in altermagnets*, Phys. Rev. B **110**, 235101 (2024), doi:[10.1103/PhysRevB.110.235101](https://doi.org/10.1103/PhysRevB.110.235101).
- [38] M. Naka, S. Hayami, H. Kusunose, Y. Yanagi, Y. Motome and H. Seo, *Anomalous Hall effect in κ -type organic antiferromagnets*, Phys. Rev. B **102**, 075112 (2020), doi:[10.1103/PhysRevB.102.075112](https://doi.org/10.1103/PhysRevB.102.075112).
- [39] M. Naka, Y. Motome and H. Seo, *Perovskite as a spin current generator*, Phys. Rev. B **103**, 125114 (2021), doi:[10.1103/PhysRevB.103.125114](https://doi.org/10.1103/PhysRevB.103.125114).
- [40] H. Reichlova, R. Lopes Seeger, R. González-Hernández, I. Kounta, R. Schlitz, D. Krieger, P. Ritzinger, M. Lammel, M. Leiviskä, A. Birk Hellenes *et al.*, *Observation of a spontaneous anomalous Hall response in the Mn_5Si_3 d-wave altermagnet candidate*, Nature Communications **15**(1), 4961 (2024), doi:[10.1038/s41467-024-48493-w](https://doi.org/10.1038/s41467-024-48493-w).
- [41] A. Hariki, Y. Takahashi and J. Kuneš, *X-ray magnetic circular dichroism in RuO_2* , Phys. Rev. B **109**, 094413 (2024), doi:[10.1103/PhysRevB.109.094413](https://doi.org/10.1103/PhysRevB.109.094413).
- [42] T. Kasuya, *A Theory of Metallic Ferro- and Antiferromagnetism on Zener's Model*, Progress of Theoretical Physics **16**(1), 45 (1956), doi:[10.1143/PTP.16.45](https://doi.org/10.1143/PTP.16.45).
- [43] K. Yosida, *Magnetic properties of Cu-Mn alloys*, Phys. Rev. **106**, 893 (1957), doi:[10.1103/PhysRev.106.893](https://doi.org/10.1103/PhysRev.106.893).
- [44] M. A. Ruderman and C. Kittel, *Indirect exchange coupling of nuclear magnetic moments by conduction electrons*, Phys. Rev. **96**, 99 (1954), doi:[10.1103/PhysRev.96.99](https://doi.org/10.1103/PhysRev.96.99).
- [45] Y.-L. Lee, *Magnetic impurities in an altermagnetic metal*, The European Physical Journal B **98**(3), 43 (2025), doi:[10.1140/epjb/s10051-025-00890-w](https://doi.org/10.1140/epjb/s10051-025-00890-w).
- [46] M. Amundsen, A. Brataas and J. Linder, *RKKY interaction in Rashba altermagnets*, Phys. Rev. B **110**, 054427 (2024), doi:[10.1103/PhysRevB.110.054427](https://doi.org/10.1103/PhysRevB.110.054427).
- [47] M. Yarmohammadi, U. Zülicke, J. Berakdar, J. Linder and J. K. Freericks, *Anisotropic light-tailored RKKY interaction in two-dimensional d-wave altermagnets*, Phys. Rev. B **111**, 224412 (2025), doi:[10.1103/k3xb-8pts](https://doi.org/10.1103/k3xb-8pts).

- [48] A. Kundu, *RKKY interaction mediated by a spin-polarized 2D electron gas with Rashba and altermagnetic coupling*, arXiv:2509.10778 (2025).
- [49] H.-J. Duan, M.-S. Fang, M.-X. Deng and R. Wang, *Néel vector and Rashba SOC effects on RKKY interaction in 2D d-wave altermagnets* (2026), [2509.26285](#).
- [50] J. J. Pla, K. Y. Tan, J. P. Dehollain, W. H. Lim, J. J. L. Morton, D. N. Jamieson, A. S. Dzurak and A. Morello, *A single-atom electron spin qubit in silicon*, Nature **489**(7417), 541 (2012), doi:[10.1038/nature11449](#).
- [51] W. Gilbert, T. Tanttu, W. H. Lim, M. Feng, J. Y. Huang, J. D. Cifuentes, S. Serrano, P. Y. Mai, R. C. C. Leon, C. C. Escott, K. M. Itoh, N. V. Abrosimov *et al.*, *On-demand electrical control of spin qubits*, Nature Nanotechnology **18**(2), 131 (2023), doi:[10.1038/s41565-022-01280-4](#).
- [52] C. Bonizzoni, A. Ghirri, F. Santanni and M. Affronte, *Quantum sensing of magnetic fields with molecular spins*, npj Quantum Information **10**(1), 41 (2024), doi:[10.1038/s41534-024-00838-5](#).
- [53] T. Hache, A. Anshu, T. Shalomayeva, G. Richter, R. Stöhr, K. Kern, J. Wrachtrup and A. Singha, *Nanoscale mapping of magnetic auto-oscillations with a single spin sensor*, Nano Letters **25**(5), 1917 (2025), doi:[10.1021/acs.nanolett.4c05531](#).
- [54] J. Wrachtrup and A. Finkler, *Single spin magnetic resonance*, Journal of Magnetic Resonance **269**, 225 (2016), doi:<https://doi.org/10.1016/j.jmr.2016.06.017>.
- [55] X. Zhao and J. Zhao, *Interlayer dzyaloshinskii-moriya interaction in spintronics*, npj Spintronics **3**(1), 25 (2025), doi:[10.1038/s44306-025-00091-2](#).
- [56] H. Padmanabhan, V. A. Stoica, P. K. Kim, M. Poore, T. Yang, X. Shen, A. H. Reid, M.-F. Lin, S. Park, J. Yang, H. H. Wang, N. Z. Koocher *et al.*, *Large exchange coupling between localized spins and topological bands in mnbi2te4*, Advanced Materials **34**(49), 2202841 (2022), doi:<https://doi.org/10.1002/adma.202202841>, <https://advanced.onlinelibrary.wiley.com/doi/pdf/10.1002/adma.202202841>.
- [57] X. Xu, B. Jiang, R. Wang, Z. Qiu, S. Guo, B. Lv and R. Zhong, *Stoichiometry-controlled structural order and tunable antiferromagnetism in Fe_xNbSe_2 ($0.05 \leq x \leq 0.38$)*, arXiv:2512.18993 (2025).
- [58] M. Yarmohammadi, S. R. Koshkaki, J. Berakdar, M. Bukov and M. H. Kolodrubetz, *Probing topological phases in a perturbed Kane-Mele model via RKKY interaction: Application to monolayer jacutingaite Pt_2HgSe_3* , Phys. Rev. B **111**, 014440 (2025), doi:[10.1103/PhysRevB.111.014440](#).
- [59] M. Yarmohammadi, M. Bukov and M. H. Kolodrubetz, *Noncollinear twisted RKKY interaction on the optically driven $\text{SnTe}(001)$ surface*, Phys. Rev. B **107**, 054439 (2023), doi:[10.1103/PhysRevB.107.054439](#).
- [60] M. Ke, M. M. Asmar and W.-K. Tse, *Nonequilibrium RKKY interaction in irradiated graphene*, Phys. Rev. Research **2**, 033228 (2020), doi:[10.1103/PhysRevResearch.2.033228](#).
- [61] M. Ke, M. M. Asmar and W.-K. Tse, *Floquet-driven indirect exchange interaction mediated by topological insulator surface states*, Phys. Rev. B **110**, 035307 (2024), doi:[10.1103/PhysRevB.110.035307](#).

- [62] S. A. A. Ghorashi and Q. Li, *Dynamical generation of higher-order spin-orbit coupling, topology, and persistent spin texture in light-irradiated altermagnets*, Phys. Rev. Lett. **135**, 236702 (2025), doi:[10.1103/tm58-lbdl](https://doi.org/10.1103/tm58-lbdl).
- [63] U. Andiel, G. D. Tsakiris, E. Cormier and K. Witte, *High-order harmonic amplitude modulation in two-colour phase-controlled frequency mixing*, Europhysics Letters **47**(1), 42 (1999), doi:[10.1209/epl/i1999-00348-5](https://doi.org/10.1209/epl/i1999-00348-5).
- [64] E. Cormier and M. Lewenstein, *Optimizing the efficiency in high order harmonic generation optimization by two-color fields*, The European Physical Journal D - Atomic, Molecular, Optical and Plasma Physics **12**(2), 227 (2000), doi:[10.1007/s100530070017](https://doi.org/10.1007/s100530070017).
- [65] I. J. Kim, C. M. Kim, H. T. Kim, G. H. Lee, Y. S. Lee, J. Y. Park, D. J. Cho and C. H. Nam, *Highly efficient high-harmonic generation in an orthogonally polarized two-color laser field*, Phys. Rev. Lett. **94**, 243901 (2005), doi:[10.1103/PhysRevLett.94.243901](https://doi.org/10.1103/PhysRevLett.94.243901).
- [66] T. T. Liu, T. Kanai, T. Sekikawa and S. Watanabe, *Significant enhancement of high-order harmonics below 10 nm in a two-color laser field*, Phys. Rev. A **73**, 063823 (2006), doi:[10.1103/PhysRevA.73.063823](https://doi.org/10.1103/PhysRevA.73.063823).
- [67] P. Wei, J. Miao, Z. Zeng, C. Li, X. Ge, R. Li and Z. Xu, *Selective enhancement of a single harmonic emission in a driving laser field with subcycle waveform control*, Phys. Rev. Lett. **110**, 233903 (2013), doi:[10.1103/PhysRevLett.110.233903](https://doi.org/10.1103/PhysRevLett.110.233903).
- [68] T. Kroh, C. Jin, P. Krogen, P. D. Keathley, A.-L. Calendron, J. P. Siqueira, H. Liang, E. L. F. ao Filho, C. D. Lin, F. X. Kärtner and K.-H. Hong, *Enhanced high-harmonic generation up to the soft X-ray region driven by mid-infrared pulses mixed with their third harmonic*, Opt. Express **26**(13), 16955 (2018), doi:[10.1364/OE.26.016955](https://doi.org/10.1364/OE.26.016955).
- [69] C. Jin, K.-H. Hong and C. D. Lin, *Optimal generation of high harmonics in the water-window region by synthesizing 800-nm and mid-infrared laser pulses*, Opt. Lett. **40**(16), 3754 (2015), doi:[10.1364/OL.40.003754](https://doi.org/10.1364/OL.40.003754).
- [70] C. Jin, G. Wang, A.-T. Le and C. D. Lin, *Route to optimal generation of soft X-ray high harmonics with synthesized two-color laser pulses*, Scientific Reports **4**(1), 7067 (2014), doi:[10.1038/srep07067](https://doi.org/10.1038/srep07067).
- [71] C. Jin, G. Wang, H. Wei, A.-T. Le and C. D. Lin, *Waveforms for optimal sub-KeV high-order harmonics with synthesized two- or three-colour laser fields*, Nature Communications **5**(1), 4003 (2014), doi:[10.1038/ncomms5003](https://doi.org/10.1038/ncomms5003).
- [72] R. Rajpoot, A. R. Holkundkar, N. Rana and G. Dixit, *Tailoring polarisation of attosecond pulses via co-rotating bicircular laser fields*, Physics Letters A **493**, 129241 (2024), doi:<https://doi.org/10.1016/j.physleta.2023.129241>.
- [73] S. Liu, O. Cohen, P. Chen and O. Neufeld, *In-plane optically tunable magnetic states in 2D materials via tailored femtosecond laser driving* (2025), [2512.14328](https://arxiv.org/abs/2512.14328).
- [74] M. Ganguli, A. Jana and A. Narayan, *Tunable topology, hall response, and spin-textures in bicircularly polarized light illuminated altermagnets*, arXiv:2509.06349 (2025).
- [75] S. Reimers, L. Odenbreit, L. Šmejkal, V. N. Strocov, P. Constantinou, A. B. Hellenes, R. Jaeschke Ubierno, W. H. Campos, V. K. Bharadwaj, A. Chakraborty *et al.*, *Direct observation of altermagnetic band splitting in CrSb thin films*, Nature Communications **15**(1), 2116 (2024), doi:[10.1038/s41467-024-46476-5](https://doi.org/10.1038/s41467-024-46476-5).

- [76] M. Grifoni and P. Hänggi, *Driven quantum tunneling*, Physics Reports **304**(5), 229 (1998), doi:[https://doi.org/10.1016/S0370-1573\(98\)00022-2](https://doi.org/10.1016/S0370-1573(98)00022-2).
- [77] G. Platero and R. Aguado, *Photon-assisted transport in semiconductor nanostructures*, Physics Reports **395**(1), 1 (2004), doi:<https://doi.org/10.1016/j.physrep.2004.01.004>.
- [78] T. Kitagawa, T. Oka, A. Brataas, L. Fu and E. Demler, *Transport properties of nonequilibrium systems under the application of light: Photoinduced quantum Hall insulators without Landau levels*, Phys. Rev. B **84**, 235108 (2011), doi:[10.1103/PhysRevB.84.235108](https://doi.org/10.1103/PhysRevB.84.235108).
- [79] T. Kitagawa, E. Berg, M. Rudner and E. Demler, *Topological characterization of periodically driven quantum systems*, Phys. Rev. B **82**, 235114 (2010), doi:[10.1103/PhysRevB.82.235114](https://doi.org/10.1103/PhysRevB.82.235114).
- [80] M. Ezawa, *Photoinduced topological phase transition and a single Dirac-cone state in silicene*, Phys. Rev. Lett. **110**, 026603 (2013), doi:[10.1103/PhysRevLett.110.026603](https://doi.org/10.1103/PhysRevLett.110.026603).
- [81] P.-H. Fu, S. Mondal, J.-F. Liu, Y. Tanaka and J. Cayao, *Floquet engineering spin triplet states in unconventional magnets*, Phys. Rev. Lett. **136**, 066703 (2026), doi:[10.1103/lkf9-jgv6](https://doi.org/10.1103/lkf9-jgv6).
- [82] P.-H. Fu, S. Mondal, J.-F. Liu and J. Cayao, *Light-induced Floquet spin-triplet Cooper pairs in unconventional magnets*, arXiv:2506.10590 (2025).
- [83] Y.-J. Wu, J. Hou, Y.-M. Li, X.-W. Luo, X. Shi and C. Zhang, *In-plane zeeman-field-induced Majorana corner and hinge modes in an s-wave superconductor heterostructure*, Phys. Rev. Lett. **124**, 227001 (2020), doi:[10.1103/PhysRevLett.124.227001](https://doi.org/10.1103/PhysRevLett.124.227001).
- [84] F. Setiawan, C.-T. Wu and K. Levin, *Full proximity treatment of topological superconductors in Josephson-junction architectures*, Phys. Rev. B **99**, 174511 (2019), doi:[10.1103/PhysRevB.99.174511](https://doi.org/10.1103/PhysRevB.99.174511).
- [85] F. Pientka, A. Keselman, E. Berg, A. Yacoby, A. Stern and B. I. Halperin, *Topological superconductivity in a planar Josephson junction*, Phys. Rev. X **7**, 021032 (2017), doi:[10.1103/PhysRevX.7.021032](https://doi.org/10.1103/PhysRevX.7.021032).
- [86] X. Huang, J. Lu, Z. Yan, M. Yan, W. Deng, G. Chen and Z. Liu, *Acoustic higher-order topology derived from first-order with built-in zeeman-like fields*, Science Bulletin **67**(5), 488 (2022), doi:<https://doi.org/10.1016/j.scib.2021.11.020>.
- [87] B. Coqblin and J. R. Schrieffer, *Exchange interaction in alloys with cerium impurities*, Phys. Rev. **185**, 847 (1969), doi:[10.1103/PhysRev.185.847](https://doi.org/10.1103/PhysRev.185.847).
- [88] H. Imamura, P. Bruno and Y. Utsumi, *Twisted exchange interaction between localized spins embedded in a one- or two-dimensional electron gas with Rashba spin-orbit coupling*, Phys. Rev. B **69**, 121303 (2004), doi:[10.1103/PhysRevB.69.121303](https://doi.org/10.1103/PhysRevB.69.121303).
- [89] J. Klinovaja and D. Loss, *RKKY interaction in carbon nanotubes and graphene nanoribbons*, Phys. Rev. B **87**, 045422 (2013), doi:[10.1103/PhysRevB.87.045422](https://doi.org/10.1103/PhysRevB.87.045422).
- [90] T. Higuchi, C. Heide, K. Ullmann, H. B. Weber and P. Hommelhoff, *Light-field-driven currents in graphene*, Nature **550**(7675), 224 (2017), doi:[10.1038/nature23900](https://doi.org/10.1038/nature23900).
- [91] Y. H. Wang, H. Steinberg, P. Jarillo-Herrero and N. Gedik, *Observation of Floquet-Bloch states on the surface of a topological insulator*, Science **342**(6157), 453 (2013), doi:[10.1126/science.1239834](https://doi.org/10.1126/science.1239834).

- [92] J. W. McIver, B. Schulte, F.-U. Stein, T. Matsuyama, G. Jotzu, G. Meier and A. Cavalleri, *Light-induced anomalous Hall effect in graphene*, Nature Physics **16**(1), 38 (2020), doi:[10.1038/s41567-019-0698-y](https://doi.org/10.1038/s41567-019-0698-y).
- [93] M. Nuske, L. Broers, B. Schulte, G. Jotzu, S. A. Sato, A. Cavalleri, A. Rubio, J. W. McIver and L. Mathey, *Floquet dynamics in light-driven solids*, Phys. Rev. Research **2**, 043408 (2020), doi:[10.1103/PhysRevResearch.2.043408](https://doi.org/10.1103/PhysRevResearch.2.043408).
- [94] Y. Liu, C. Yang, G. Gaertner, J. Huckabee, A. V. Suslov, G. Refael, F. Nathan, C. Lewandowski, L. E. F. Foa Torres, I. Esin *et al.*, *Signatures of Floquet electronic steady states in graphene under continuous-wave mid-infrared irradiation*, Nature Communications **16**(1), 2057 (2025), doi:[10.1038/s41467-025-57335-2](https://doi.org/10.1038/s41467-025-57335-2).
- [95] See videos in the Supplemental Material at [URL will be inserted by publisher] for the critical single- and two-color Floquet \mathcal{A}_c and \mathcal{S}_c .
- [96] H. Niu, H. Y. Kwon, T. Ma, Z. Cheng, C. Ophus, B. Miao, L. Sun, Y. Wu, K. Liu, S. S. P. Parkin, C. Won, A. K. Schmid *et al.*, *Reducing crystal symmetry to generate out-of-plane Dzyaloshinskii–Moriya interaction*, Nature Communications **15**(1), 10199 (2024), doi:[10.1038/s41467-024-54521-6](https://doi.org/10.1038/s41467-024-54521-6).
- [97] R. E. Camley and K. L. Livesey, *Consequences of the Dzyaloshinskii–Moriya interaction*, Surface Science Reports **78**(3), 100605 (2023), doi:<https://doi.org/10.1016/j.surfrep.2023.100605>.
- [98] M. Hoffmann, B. Zimmermann, G. P. Müller, D. Schürhoff, N. S. Kiselev, C. Melcher and S. Blügel, *Antiskyrmions stabilized at interfaces by anisotropic Dzyaloshinskii–Moriya interactions*, Nature Communications **8**(1), 308 (2017), doi:[10.1038/s41467-017-00313-0](https://doi.org/10.1038/s41467-017-00313-0).
- [99] E. Y. Vedmedenko, P. Riego, J. A. Arregi and A. Berger, *Interlayer Dzyaloshinskii–Moriya interactions*, Phys. Rev. Lett. **122**, 257202 (2019), doi:[10.1103/PhysRevLett.122.257202](https://doi.org/10.1103/PhysRevLett.122.257202).
- [100] Q. Zhang, J. Liang, K. Bi, L. Zhao, H. Bai, Q. Cui, H.-A. Zhou, H. Bai, H. Feng, W. Song, G. Chai, O. Gladii *et al.*, *Quantifying the Dzyaloshinskii–Moriya interaction induced by the bulk magnetic asymmetry*, Phys. Rev. Lett. **128**, 167202 (2022), doi:[10.1103/PhysRevLett.128.167202](https://doi.org/10.1103/PhysRevLett.128.167202).
- [101] M. Robertson, C. J. Agostino, G. Chen, S. P. Kang, A. Mascaraque, E. Garcia Michel, C. Won, Y. Wu, A. K. Schmid and K. Liu, *In-plane néel wall chirality and orientation of interfacial Dzyaloshinskii–Moriya vector in magnetic films*, Phys. Rev. B **102**, 024417 (2020), doi:[10.1103/PhysRevB.102.024417](https://doi.org/10.1103/PhysRevB.102.024417).
- [102] R. Allenspach, A. Bischof, B. Boehm, U. Drechsler, O. Reich, M. Sousa, S. Tacchi and G. Carlotti, *Dzyaloshinskii–Moriya interaction in Ni/Cu(001)*, Phys. Rev. B **110**, 014402 (2024), doi:[10.1103/PhysRevB.110.014402](https://doi.org/10.1103/PhysRevB.110.014402).
- [103] B. Jiang, M. Hu, J. Bai, Z. Song, C. Mu, G. Qu, W. Li, W. Zhu, H. Pi, Z. Wei *et al.*, *A metallic room-temperature d-wave altermagnet*, Nature Physics **21**, 754 (2025), doi:[10.1038/s41567-025-02822-y](https://doi.org/10.1038/s41567-025-02822-y).
- [104] F. Zhang, X. Cheng, Z. Yin, C. Liu, L. Deng, Y. Qiao, Z. Shi, S. Zhang, J. Lin, Z. Liu *et al.*, *Crystal-symmetry-paired spin–valley locking in a layered room-temperature metallic altermagnet candidate*, Nature Physics **21**(5), 760 (2025), doi:[10.1038/s41567-025-02864-2](https://doi.org/10.1038/s41567-025-02864-2).

- [105] M. Weber, S. Wust, L. Haag, A. Akashdeep, K. Leckron, C. Schmitt, R. Ramos, T. Kikkawa, E. Saitoh, M. Kläui, L. Šmejkal, J. Sinova *et al.*, *All optical excitation of spin polarization in d-wave altermagnets* (2024), [2408.05187](#).
- [106] O. Fedchenko, J. Minár, A. Akashdeep, S. W. D'Souza, D. Vasilyev, O. Tkach, L. Odenbreit, Q. Nguyen, D. Kutnyakhov, N. Wind *et al.*, *Observation of time-reversal symmetry breaking in the band structure of altermagnetic RuO₂*, *Science Advances* **10**(5), eadj4883 (2024), doi:[10.1126/sciadv.adj4883](#).
- [107] P. Wahl, P. Simon, L. Diekhöner, V. S. Stepanyuk, P. Bruno, M. A. Schneider and K. Kern, *Exchange interaction between single magnetic adatoms*, *Phys. Rev. Lett.* **98**, 056601 (2007), doi:[10.1103/PhysRevLett.98.056601](#).